human cancers due to a process of long-range epigenetic silencing, has recently attracted attention.[33] Therefore, we used a custom-made BAC array[20] that may be suitable for gaining an overview of the DNA methylation status of individual large regions among all chromosomes (Table S4), and for obtaining reproducible diagnostic indicators. In fact we have successfully obtained optimal indicators for carcinogenetic risk estimation and prognostication of renal cell carcinomas[23] and hepatocellular carcinomas[34] by BAMCA using the same array as that employed in this study. On the other hand, we must pay attention to the quantitative accuracy of BAMCA, because it is a PCR-based method differing from other genome-wide DNA methylation analyses not using PCR, such as the methylated DNA immunoprecipitation-microarray. In order to validate the results of BAMCA, we quantitatively evaluated the DNA methylation status of each Xma I/Sma I site yielding labeled products which are effective in BAMCA on representative BAC clones, by pyrosequencing. As shown in the example in Figure S1 and Table S5, pyrosequencing validated the BAMCA data on the representative BAC clone.

The present DNA methylation analysis revealed that stepwise DNA methylation alterations during urothelial carcinogenesis occurred in a genome-wide manner (Fig. 1). We then performed unsupervised hierarchical clustering analysis based on the genome-wide DNA methylation status of noncancerous urothelia, and as a result, 17 patients were subclassified into Clusters $A_N$ and $B_N$. Corresponding UCs showing deeper invasion were found to be accumulated in Cluster $B_N$. Genome-wide DNA methylation profiles of noncancerous urothelia obtained from patients with invasive UCs were inherited by the invasive UCs themselves (Fig. 2b). DNA methylation profiles of noncancerous urothelia obtained from patients with superficial UCs were not always inherited by superficial UCs (data not shown), corresponding to the alternative malignant progression of superficial papillary carcinoma to nodular invasive carcinoma, via papillonodular carcinoma. Genome-wide DNA methylation alterations that were correlated with the development of more malignant invasive cancers were already accumulated in noncancerous urothelia, suggesting that DNA methylation alterations at the precancerous stage may not occur randomly but are prone to further accumulation of genetic and epigenetic alterations and generate more malignant cancers.

The present genome-wide analysis revealed DNA methylation profiles that were able to completely discriminate noncancerous urothelia obtained from patients with UCs from normal urothelia and diagnose them as having a high risk of urothelial carcinogenesis with a sensitivity and specificity of 100%. We are currently attempting to develop methodology for assessing the tendency for DNA methylation in the 83 BAC regions in urine samples with a view to application for screening of healthy individuals. If it proves possible to identify individuals who are at high risk of urothelial carcinogenesis, then strategies for the prevention or early detection of UCs, such as smoking cessation or repeated urine cytology examinations, might be applicable.

Even after surgery with curative intent, some UCs relapse and metastasize to lymph nodes or distant organs.[35] Recently, new systemic chemotherapy and targeted therapy have been developed for treatment for UCs.[36] In order to start adjuvant systemic chemotherapy immediately in patients who have undergone surgery and are still at high risk of recurrence and metastasis, prognostic indicators have been explored. The present genome-wide analysis revealed DNA methylation profiles that were able to discriminate patients who suffered recurrence after surgery from patients who did not with a sensitivity and specificity of 100% (Fig. 4b), whereas a high histological grade,[21] invasive growth (pT2 or more), and vascular or lymphatic involvement, which are known to have a prognostic impact,[37,38] were incapable of such complete discrimination (data not shown). Therefore, a combination of the 20 BAC clones can have significant prognostic value for patients with UCs. Since a sufficient quantity of good-quality DNA can be obtained from each surgical specimen, our array-based analysis that overviews aberrant DNA methylation of each BAC region is immediately applicable to routine laboratory examinations for prognostication after surgery. The reliability of such prognostication will need to be validated in a prospective study.

As mentioned above, UCs are remarkable because of their multicentricity. Approximately 10–30% of patients with UCs of the renal pelvis and ureter develop intravesical metachronous UCs after nephroureterectomy.[24,25] Therefore, such patients have to undergo repeated urethrocystoscopic examinations to detect intravesical metachronous UCs. To decrease the need for invasive urethrocystoscopic examinations and assist close follow-up of such patients after nephroureterectomy, indicators for intravesical metachronous UCs have been needed. All of our patients who developed intravesical metachronous UCs after nephroureterectomy belonged to Cluster $B_{NP}$, indicating that DNA methylation profiles of noncancerous urothelia obtained by nephroureterectomy from patients with UCs of the renal pelvis or ureter, which may be exposed to the same carcinogens in the urine as noncancerous urothelia from which metachronous UCs originate, are correlated with the risk of intravesical metachronous UC development. The present genome-wide analysis revealed DNA methylation profiles that were able to completely discriminate patients with UCs of the renal pelvis or ureter who developed intravesical metachronous UCs from patients who did not, in noncancerous urothelia from nephroureterectomy specimens. A combination of the present 11 BAC clones may be an optimal indicator for the development of intravesical metachronous UC. The reliability of such prognostication will again need to be validated in a prospective study.

With respect to background factors of genome-wide DNA methylation alterations during urothelial carcinogenesis, smoking history did not correlate significantly with the numbers of BAC clones showing DNA hypo- or hypermethylation in noncancerous urothelia obtained from patients with UCs and in UCs, or with clustering (Cluster $A_N$ *vs* Cluster $B_N$ and Cluster $A_T$ *vs* Cluster $B_T$) (Table S6). In addition, immunohistochemically examined DNMT1 protein expression levels did not correlate significantly with the numbers of BAC clones showing DNA hypo- or hypermethylation in noncancerous urothelia obtained from patients with UCs and in UCs, or with clustering (Cluster $A_N$ *vs* Cluster $B_N$ and Cluster $A_T$ *vs* Cluster $B_T$) (Table S7), indicating that expression levels of DNMT1 did not by themselves simply determine DNA methylation profiles. However, our previous study revealed remarkable protein overexpression of DNMT1 in noncancerous urothelia obtained from patients with UCs as compared to normal urothelia.[8] Therefore, undefined cofactors may recruit DNMT1 or other proteins regulating DNA methylation status to aberrant target sequences and may participate in DNA methylation alterations in noncancerous urothelia obtained from patients with UCs. Further studies are needed to elucidate molecular mechanisms of DNA methylation alterations in such noncancerous urothelia.

Moreover, when the DNA methylation status for CpG islands of *p16*, human MutL homologue 1 (*hMLH1*), thrombospondin-1 (*THBS-1*), and death-associated protein kinase (*DAPK*) genes and the methylated in tumor (MINT)-1, -2, -12, -25, and -31 clones were examined in noncancerous urothelia obtained from patients with UCs and in UCs by methylation-specific PCR and combined bisulfite restriction enzyme analysis as in our previous study,[9,39] the incidence of DNA


doi: 10.1111/j.1349-7006.2009.01330.x

methylation on each CpG island and the average number of methylated CpG islands did not correlate significantly with the numbers of BAC clones showing DNA hypo- or hypermethylation in noncancerous urothelia obtained from patients with UCs and in UCs, or with clustering (Cluster $A_N$ *vs* Cluster $B_N$ and Cluster $A_T$ *vs* Cluster $B_T$) (Table S8). Therefore, molecular mechanisms for alterations of genome-wide DNA methylation profiles may differ from those for regional DNA hypermethylation on CpG islands.

Although BAMCA mainly provides an overview of the DNA methylation status of individual large regions among all chromosomes as mentioned above, it may also be able to identify genes for which expressions are regulated by DNA methylation, since there are promoter regions of specific genes including CpG islands on BAC clones showing clinicopathologically significant DNA hypo- or hypermethylation (Table S4). Expression levels and the DNA methylation status of these genes, as well as the functions of the proteins coded by such genes, will be examined in a future investigation. If further studies identify tumor-related genes for which expression levels are regulated by DNA methylation among such candidates, these tumor-related genes may serves as targets for epigenetic prevention and therapy, along with the molecules causing alterations of genome-wide DNA methylation profiles.

## Acknowledgments

This study was supported by a Grant-in-Aid for the Third Term Comprehensive 10-Year Strategy for Cancer Control from the Ministry of Health, Labor and Welfare of Japan; a Grant-in-Aid for Cancer Research from the Ministry of Health, Labor and Welfare of Japan; a Grant from the New Energy and Industrial Technology Development Organization (NEDO); and the Program for Promotion of Fundamental Studies in Health Sciences of the National Institute of Biomedical Innovation (NiBio). N. Nishiyama is an awardee of a research resident fellowship from the Foundation for Promotion of Cancer Research in Japan.

## References

1 Jones PA, Baylin SB. The fundamental role of epigenetic events in cancer. *Nat Rev Genet* 2002; **3**: 415–28.
2 Eden A, Gaudet F, Waghmare A, Jaenisch R. Chromosomal instability and tumors promoted by DNA hypomethylation. *Science* 2003; **300**: 455.
3 Baylin SB, Ohm JE. Epigenetic gene silencing in cancer – a mechanism for early oncogenic pathway addiction? *Nat Rev Cancer* 2006; **6**: 107–16.
4 Gronbaek K, Hother C, Jones PA. Epigenetic changes in cancer. *Apmis* 2007; **115**: 1039–59.
5 Feinberg AP. Phenotypic plasticity and the epigenetics of human disease. *Nature* 2007; **447**: 433–40.
6 Kanai Y, Hirohashi S. Alterations of DNA methylation associated with abnormalities of DNA methyltransferases in human cancers during transition from a precancerous to a malignant state. *Carcinogenesis* 2007; **28**: 2434–42.
7 Kanai Y. Alterations of DNA methylation and clinicopathological diversity of human cancers. *Pathol Int* 2008; **58**: 544–8.
8 Nakagawa T, Kanai Y, Saito Y, Kitamura T, Kakizoe T, Hirohashi S. Increased DNA methyltransferase 1 protein expression in human transitional cell carcinoma of the bladder. *J Urol* 2003; **170**: 2463–6.
9 Nakagawa T, Kanai Y, Ushijima S, Kitamura T, Kakizoe T, Hirohashi S. DNA hypermethylation on multiple CpG islands associated with increased DNA methyltransferase DNMT1 protein expression during multistage urothelial carcinogenesis. *J Urol* 2005; **173**: 1767–71.
10 Nakagawa T, Kanai Y, Ushijima S, Kitamura T, Kakizoe T, Hirohashi S. DNA hypomethylation on pericentromeric satellite regions significantly correlates with loss of heterozygosity on chromosome 9 in urothelial carcinomas. *J Urol* 2005; **173**: 243–6.
11 Kakizoe T, Tobisu K, Takai K, Tanaka Y, Kishi K, Teshima S. Relationship between papillary and nodular transitional cell carcinoma in the human urinary bladder. *Cancer Res* 1998; **48**: 2299–303.
12 Kakizoe T. Development and progression of urothelial carcinoma. *Cancer Sci* 2006; **97**: 821–8.
13 Aleman A, Adrien L, Lopez-Serra L *et al.* Identification of DNA hypermethylation of SOX9 in association with bladder cancer progression using CpG microarrays. *Br J Cancer* 2008; **98**: 466–73.
14 Estecio MR, Yan PS, Ibrahim AE *et al.* High-throughput methylation profiling by MCA coupled to CpG island microarray. *Genome Res* 2007; **17**: 1529–36.
15 Jacinto FV, Ballestar E, Ropero S, Esteller M. Discovery of epigenetically silenced genes by methylated DNA immunoprecipitation in colon cancer cells. *Cancer Res* 2007; **67**: 11481–6.
16 Nielander I, Bug S, Richter J, Giefing M, Martin-Subero JI, Siebert R. Combining array-based approaches for the identification of candidate tumor suppressor loci in mature lymphoid neoplasms. *Apmis* 2007; **115**: 1107–34.
17 Misawa A, Inoue J, Sugino Y *et al.* Methylation-associated silencing of the nuclear receptor I2 gene in advanced-type neuroblastomas, identified by bacterial artificial chromosome array-based methylated CpG island amplification. *Cancer Res* 2005; **65**: 10233–42.
18 Sugino Y, Misawa A, Inoue J *et al.* Epigenetic silencing of prostaglandin E receptor 2 (PTGER2) is associated with progression of neuroblastomas. *Oncogene* 2007; **26**: 7401–13.
19 Tanaka K, Imoto I, Inoue J *et al.* Frequent methylation-associated silencing of a candidate tumor-suppressor, CRABP1, in esophageal squamous-cell carcinoma. *Oncogene* 2007; **26**: 6456–68.
20 Inazawa J, Inoue J, Imoto I. Comparative genomic hybridization (CGH)-arrays pave the way for identification of novel cancer-related genes. *Cancer Sci* 2004; **95**: 559–63.
21 Lopez-Beltran A, Sauter G, Gasser T *et al.* Tumours of the urinary system. In: ed. Eble JN, Sauter G, Epstein JI, Sesterhenn IA. *World Health Organization classification of tumours. Pathology and genetics. Tumours of the urinary system and male genital organs*. Lyon: IARC Press, 2004; 89–157.
22 Illingworth R, Kerr A, Desousa D *et al.* A novel CpG island set identifies tissue-specific methylation at developmental gene loci. *PLoS Biol* 2008; **6**: e22.
23 Arai E, Ushijima S, Fujimoto H *et al.* Genome-wide DNA methylation profiles in both precancerous conditions and clear cell renal cell carcinomas are correlated with malignant potential and patient outcome. *Carcinogenesis* 2009; **30**: 214–21.
24 Manabe D, Saika T, Ebara S *et al.* Comparative study of oncologic outcome of laparoscopic nephroureterectomy and standard nephroureterectomy for upper urinary tract transitional cell carcinoma. *Urology* 2007; **69**: 457–61.
25 Hall MC, Womack S, Sagalowsky AI, Carmody T, Erickstad MD, Roehrborn CG. Prognostic factors, recurrence, and survival in transitional cell carcinoma of the upper urinary tract: a 30-year experience in 252 patients. *Urology* 1998; **52**: 594–601.
26 Harris AL, Neal DE. Bladder cancer – field versus clonal origin. *N Engl J Med* 1992; **326**: 759–61.
27 Maruyama R, Toyooka S, Toyooka KO *et al.* Aberrant promoter methylation profile of bladder cancer and its relationship to clinicopathological features. *Cancer Res* 2001; **15**: 8659–63.
28 Sathyanarayana UG, Maruyama R, Padar A *et al.* Molecular detection of noninvasive and invasive bladder tumor tissues and exfoliated cells by aberrant promoter methylation of laminin-5 encoding genes. *Cancer Res* 2004; **15**: 1425–30.
29 Catto JW, Azzouzi AR, Rehman I *et al.* Promoter hypermethylation is associated with tumor location, stage, and subsequent progression in transitional cell carcinoma. *J Clin Oncol* 2005; **23**: 2903–10.
30 Yates DR, Rehman I, Abbod MF *et al.* Promoter hypermethylation identifies progression risk in bladder cancer. *Clin Cancer Res* 2007; **13**: 2046–2053.
31 Kim EJ, Kim YJ, Jeong P, Ha YS, Bae SC, Kim WJ. Methylation of the RUNX3 promoter as a potential prognostic marker for bladder tumor. *J Urol* 2008; **180**: 1141–5.
32 Maekita T, Nakazawa K, Mihara M *et al.* High levels of aberrant DNA methylation in Helicobacter pylori-infected gastric mucosae and its possible association with gastric cancer risk. *Clin Cancer Res* 2006; **12**: 989–95.
33 Frigola J, Song J, Stirzaker C, Hinshelwood RA, Peinado MA, Clark SJ. Epigenetic remodeling in colorectal cancer results in coordinate gene suppression across an entire chromosome band. *Nat Genet* 2006; **38**: 540–9.
34 Arai E, Ushijima S, Gotoh M *et al.* Genome-wide DNA methylation profiles in liver tissue at the precancerous stage and in hepatocellular carcinoma. *Int J Cancer* 2009; (in press).

35 Stein JP, Lieskovsky G, Cote R *et al.* Radical cystectomy in the treatment of invasive bladder cancer: long-term results in 1,054 patients. *J Clin Oncol* 2001; **19**: 666–75.
36 Gallagher DJ, Milowsky MI, Bajorin DF. Advanced bladder cancer: status of first-line chemotherapy and the search for active agents in the second-line setting. *Cancer* 2008; **113**: 1284–93.
37 Lipponen PK. The prognostic value of basement membrane morphology, tumour histology and morphometry in superficial bladder cancer. *J Cancer Res Clin Oncol* 1993; **119**: 295–300.
38 Scrimger RA, Murtha AD, Parliament MB *et al.* Muscle-invasive transitional cell carcinoma of the urinary bladder: a population-based study of patterns of care and prognostic factors. *Int J Radiat Oncol Biol Phys* 2001; **51**: 23–30.
39 Etoh T, Kanai Y, Ushijima S *et al.* Increased DNA methyltransferase 1 (DNMT1) protein expression correlates significantly with poorer tumor differentiation and frequent DNA hypermethylation of multiple CpG islands in gastric cancers. *Am J Pathol* 2004; **164**: 689–99.

## Supporting Information

Additional Supporting Information may be found in the online version of this article:

**Fig. S1.** Examples of bacterial artificial chromosome (BAC) array-based methylated CpG island amplification (BAMCA) data validation by pyrosequencing.

**Table S1.** Eighty-three bacterial artificial chromosome (BAC) clones that were able to discriminate noncancerous urothelia obtained from patients with urothelial carcinomas (UCs) (N) from normal urothelia (C) with a sensitivity and specificity of 75% or more.

**Table S2.** Twenty bacterial artificial chromosome (BAC) clones that were able to discriminate urothelial carcinomas (UCs) in patients who developed recurrence (Pos) from those in patients who did not (Neg).

**Table S3.** Eleven bacterial artificial chromosome (BAC) clones that were able to discriminate noncancerous urothelia in patients with urothelial carcinomas (UCs) of the renal pelvis or ureter who developed intravesical metachronous UC (Pos) from those in patients who did not (Neg).

**Table S4.** Genes, CpG islands in the promoter regions, and repeat elements of bacterial artificial chromosome (BAC) clones in Tables S1, S2, and S3.

**Table S5.** Primer sets for validation study by pyrosequencing.

**Table S6.** Correlation between smoking history and DNA methylation status in noncancerous urothelia obtained from patients with urothelial carcinomas (UCs) and UCs.

**Table S7.** Correlation between protein expression levels of DNA methyltransferase (DNMT) 1 and DNA methylation status in noncancerous urothelia obtained from patients with urothelial carcinomas (UCs) and UCs.

**Table S8.** Correlation between regional DNA hypermethylation on CpG islands and the results of bacterial artificial chromosome (BAC) array-based methylated CpG island amplification (BAMCA) in noncancerous urothelia obtained from patients with urothelial carcinomas (UCs) and UCs.

Please note: Wiley-Blackwell are not responsible for the content or functionality of any supporting materials supplied by the authors. Any queries (other than missing material) should be directed to the corresponding author for the article.



doi: 10.1111/j.1349-7006.2009.01330.x

Cancer Science
The official journal of the Japanese Cancer Association JCA

# Establishment of six new human biliary tract carcinoma cell lines and identification of MAGEH1 as a candidate biomarker for predicting the efficacy of gemcitabine treatment

Hidenori Ojima,[1] Daitaro Yoshikawa,[2] Yoshihiro Ino,[1] Hiroko Shimizu,[2] Masashi Miyamoto,[2] Akiko Kokubu,[2] Nobuyoshi Hiraoka,[1] Noriaki Morofuji,[3] Tadashi Kondo,[3] Hiroaki Onaya,[4] Takuji Okusaka,[5] Kazuaki Shimada,[6] Yoshihiro Sakamoto,[6] Minoru Esaki,[6] Satoshi Nara,[6] Tomoo Kosuge,[6] Setsuo Hirohashi,[1,2] Yae Kanai[1] and Tatsuhiro Shibata[1,2,7]

[1]Pathology Division, [2]Cancer Genomics Project, [3]Proteome Bioinformatics Project, National Cancer Center Research Institute, Chuo-ku, Tokyo; [4]Diagnostic Radiology Section, Clinical Trials and Practice Support Division, Center for Cancer Control and Information Services, National Cancer Center, Chuo-ku, Tokyo; [5]Hepatobiliary and Pancreatic Oncology Division, [6]Hepatobiliary and Pancreatic Surgery Division, National Cancer Center Hospital, Chuo-ku, Tokyo, Japan

(Received October 6, 2009/Revised November 25, 2009; December 1, 2009/Accepted December 1, 2009/Online publication January 21, 2010)

**The aim of this study was to establish new biliary tract carcinoma (BTC) cell lines and identify predictive biomarkers for the potential effectiveness of gemcitabine therapy. Surgical specimens of BTC were transplanted directly into immunodeficient mice to establish xenografts, then subjected to *in vitro* cell culture. The gemcitabine sensitivity of each cell line was determined and compared with the genome-wide gene expression profile. A new predictive biomarker candidate was validated using an additional cohort of gemcitabine-treated BTC cases. From 55 BTC cases, we established 19 xenografts and six new cell lines. Based on their gemcitabine sensitivity, 10 BTC cell lines (including six new and four publicly available ones) were clearly categorized into two groups, and MAGEH1 mRNA expression in the tumor cells showed a significant negative correlation with their sensitivity to gemcitabine. Immunohistochemically, MAGEH1 protein was detected in three (50%) out of six sensitive cell lines, and four (100%) out of four resistant cell lines. In the validation cohort of gemcitabine-treated recurrence cases, patients were categorized into "effective" and "non-effective" groups according to the RECIST guidelines for assessment of chemotherapeutic effects. MAGEH1 protein expression was detected in two (40%) out of five "effective" cases and all four (100%) "non-effective" cases. We have established a new BTC bioresource that covers a wide range of biological features, including drug sensitivity, and is linked with clinical information. Negative expression of MAGEH1 protein serves as a potential predictive marker for the effectiveness of gemcitabine therapy in BTC. (*Cancer Sci* 2010; 101: 882–888)**

Biliary tract carcinoma (BTC) has a poor prognosis, and most cases are diagnosed at advanced stages when patients present with overt symptoms. Previous studies have reported that surgical resection is the only curative treatment for BTC patients,[1–4] and no standard chemotherapy regimens have been established for inoperable cases or cases of recurrence after surgical resection.[5,6] Exceptionally, gemcitabine (2′-deoxy-2′-difluorodeoxycytidine), a deoxycytidine analog with structural and metabolic similarities to cytarabine, has been reported to be clinically effective and is considered a first-line chemotherapy for BTC, although its associated response rates (8–60%) and median overall survival (6.3–16 months) are not satisfactory.[7] It has been reported that both intrinsic and acquired resistance are important factors in the failure of gemcitabine treatment in patients with pancreatic cancer.[8] However, there have been few attempts to clarify the molecular mechanisms of gemcitabine resistance, and no data are currently available for BTC.

One factor preventing better understanding of drug resistance at the cellular and molecular levels in BTC is that only a few BTC cell lines are available for such analyses. Additionally, the construction and utility of an animal experimental model is essential for validating the *in vitro* data for these cell lines, but no such model has been established. Therefore, there is an urgent need to establish BTC cell lines from a wide range of clinical cases and apply them for translational research aimed at connecting basic research with clinical trials. In the present study, we successfully prepared 19 xenograft models from surgically resected BTC samples, and established six new cell lines. Using these new resources, we searched for molecular biomarkers associated with gemcitabine sensitivity. We also validated the efficacy of one candidate molecule, MAGEH1, as a surrogate biomarker of gemcitabine response by immunohistochemical analysis of an additional clinical cohort of gemcitabine-treated BTC.

## Materials and Methods

**Establishment of xenografts and tumor cell lines.** The study included 55 patients with BTC who underwent radical surgery with curative intent at the National Cancer Center Hospital (Tokyo, Japan) between 2005 and 2008. The main tumor nodule was located in the lower, middle, and upper thirds of the extrahepatic bile duct, the hilar bile duct, and intrahepatic area in 4, 11, 2, 4, and 34 patients, respectively. Tumor specimens were transported to the Surgical Pathology department immediately after surgical resection, and tissue in excess of that needed for diagnosis was used for this study. The tumor tissues were washed in physiological saline, cut into small pieces (2–4 $mm^3$ fragments), then implanted subcutaneously into SCID mice. Congenital athymic female C.B17/Icr-scid(scid/scid) mice (CLEA Japan, Tokyo, Japan), 5–7 weeks old, were bred and housed under specific pathogen-free conditions at the National Cancer Center Research Institute Animal Center. Tumor growth to a size of 1–2 cm after maintaining the animals for 1–2 months was regarded as engraftment, and the tumors were passaged a maximum of three to five times. Xenografts in mice were passaged similarly to the transplantation of surgical

[7]To whom correspondence should be addressed. E-mail: tashibat@ncc.go.jp



doi: 10.1111/j.1349-7006.2009.01462.x

specimens, and the tumors were subjected to cell culture after each passage. For establishment of cell lines, the xenograft tumor tissues were washed in Isozin (Meiji, Tokyo, Japan) and physiological saline, cut into small pieces, then plated into 6 cm dishes containing RPMI medium supplemented with 10% FC), 2 mM L-glutamine, 100 mg/mL streptomycin sulfate, and 100 ID/mL penicillin G sodium. Some surgical specimens were directly subjected to cell line preparation. Contaminating fibroblasts were periodically removed by wiping under microscopic observation. The cells were incubated at 37°C in 5% $CO_2$ in air, and the medium was changed once or twice a week. A solution of 0.05% trypsin and 0.53 mM EDTA (1×; Gibco™/Invitrogen Corporation, Carlsbad, CA, USA) was used for passaging the cells (1:3 split). Each cell line underwent repeated passage more than 20 times. Established cell lines were implanted subcutaneously into SCID mice to make xenografts for further analyses.

Mice were kept at the Animal Care and Use Facilities of the National Cancer Center (Tokyo, Japan) under specific pathogen-free conditions. All experiments were approved by the Animal Care and Ethics Committee of the National Cancer Center. This study was approved by the Ethical Committee of the National Cancer Center.

**Biliary tract carcinoma cell lines obtained from cell banks.** Four human BTC cell lines derived from Japanese patients (TKKK, OZ, TGBC24TKB, and HuCCT1) were purchased from Riken Bioresource Center (Tsukuba, Japan) or from the Japanese Collection of Research Bioresources (Osaka, Japan). The TKKK cell line was derived from intrahepatic cholangiocarcinoma, and the OZ, TGBC24TKB, and HuCCT1 cell lines from extrahepatic bile duct carcinoma.

**Chemicals.** Gemcitabine was obtained from Eli Lilly Pharmaceuticals (Indianapolis, IN, USA). All other chemicals were of analytical grade and commercially available.

**Cytotoxicity assays for gemcitabine.** The cytotoxicity of gemcitabine for each cell line was assessed by a modified 3-(4,5-dimethylthiazol-2-yl)-5-(3-carboxymethoxyphenyl)-2-(4-sulfophenyl)-2H-tetrazolium, inner salt assay with CellTiter 96 AQueous One Solution Reagent (Promega, Madison, WI, USA). Tumor cells (2000 cells/well) in the exponential growth phase were grown in 96-well plates. Twenty-four hours after plating, the cells were incubated in the presence of each concentration (0 (control)–100 μM) of gemcitabine for another 72 h at 37°C in a humidified atmosphere of 5% $CO_2$ in air. After treatment, 20 μL CellTiter 96 AQueous One Solution Reagent was dropped into each well in the plates and the absorbance at 490 nm was recorded. Absorbance values were expressed as a percentage of untreated controls, and $IC_{50}$ was calculated.

**Gene expression analysis.** Total RNA was extracted from 10 BTC cell lines using an RNeasy Micro Kit (Qiagen, Velencia, CA, USA) in accordance with the manufacturer's instructions. The total RNA yields and purity were determined spectrophotometrically by measuring the absorbance of aliquots at 260 and 280 nm. cDNA and Cy3-labeled cRNA were synthesized using a Quick Amp Labeling Kit (Agilent Technologies, Santa Clara, CA, USA). The labeled cRNA probe was hybridized to an oligonucleotide microarray (Whole Human Genome 44K Array; Agilent Technologies) covering more than 41 000 human transcripts. Array hybridization and washing were carried out according to the recommended protocols, and microarrays were scanned using a DNA Microarray Scanner (Agilent Technologies) and analyzed using Gene Spring software (Agilent Technologies).

**Quantitative RT-PCR.** One microgram of total RNA was converted to cDNA using a Transcriptor First Strand cDNA Synthesis Kit (Roche, Basel, Switzerland) in accordance with the manufacturer's instructions. Quantitative RT-PCR (qRT-PCR) was carried out using LightCycler 480 (Roche) in accordance with the manufacturer's instructions. For standardization of the amount of RNA, expression of GAPDH in each sample was quantified. (Primers are shown in Table S1.)

**Mutation analysis of *p53* and *KRAS* genes.** Each exon of the *p53* and *KRAS* genes (exons 5–8 of *p53* and exons 1–2 of *KRAS*) was amplified from genomic DNA of each cell line and gel-purified. Direct sequencing was carried out using a BigDye Terminator v3.1 Cycle Sequencing Kit (Applied Biosystems, Foster City, California, USA). (Primers are shown in Table S1.)

**Assessment of response to gemcitabine in cases of recurrent BTC.** Among the 100 patients who underwent surgery for BTC between September 26, 2003, and October 2, 2007, 34 developed recurrent tumors and received chemotherapy, and were followed for 6 months or longer. Among these patients, 24 who were treated with gemcitabine alone were selected for this study. The mean duration of postoperative follow-up in these 24 patients was 627 days. We further excluded 15 patients from the analysis because: (i) the drug administration period was less than 1 month in three patients; (ii) the diagnosis of tumor recurrence was not consistent between the oncologist and the radiologist in three patients; (iii) we were unable to obtain an accurate judgement of the efficacy of gemcitabine treatment in five patients; (iv) the histological diagnosis was an uncommon type of adenocarcinoma (bile duct cystadenocarcinoma, solid adenocarcinoma, and combined carcinoma) in three patients; and (v) preoperative therapy (radiation therapy) had been carried out in one patient. The effect of chemotherapy was assessed by an oncologist and a radiologist (T.O. and H.O., respectively) in accordance with the RECIST guidelines for assessment of chemotherapeutic effects.[9] None of the patients was judged as showing a complete response or a partial response. The effect of chemotherapy was categorized as "effective" or "non-effective". The "effective" group included patients whose efficacy state was stable disease for 6 months or more during chemotherapy. The "non-effective" group included patients whose efficacy state was stable disease for 5 months or less, or progressive disease during chemotherapy.

**Immunohistochemical reactivity of MAGEH1 in human tumor xenografts and surgically resected specimens.** Immunohistochemical analysis of MAGEH1 expression on formalin-fixed, paraffin-embedded sections of tumor xenograft tissues and surgical specimens was done using the polymer-based method (Envision+Dual Link System-HRP; Dako, Glostrup, Denmark) in accordance with the manufacturer's instructions. For antigen retrieval, the sections were autoclaved in 10 mM citrate buffer (pH 6.0) at 121°C for 10 min. We used a rabbit anti-MAGEH1 polyclonal antibody (ab64784; Abcom, Cambridge, Massachusetts, USA) at a dilution of 1:500. Staining intensity was independently evaluated by two pathologists (H.O. and T.S.) without knowledge of the clinical data. Using the expression in normal hepatocytes or pancreatic duct epithelial cells as a positive control, we classified cases as MAGEH1-positive when more than 50% of tumor cells were positively stained. If the tumor showed varying degrees of differentiation, staining intensity was evaluated in the area with the most dominant type of differentiation.

**Statistical analysis.** The unpaired *t*-test was used for assessment of the microarray data. Microarray and qRT-PCR data were analyzed by Pearson's correlation test.

## Results

**Establishment and characterization of BTC xenografts and cell lines.** To establish useful BTC resources, we subcutaneously transplanted 55 BTC samples (4, 11, 2, 4, and 34 cases of lower, middle, and upper thirds of the extrahepatic bile duct carcinoma, hilar bile duct carcinoma, and intrahepatic cholangiocarcinoma, respectively) into 435 immunocompromised (SCID) mice.

**Table 1. Clinicopathological features of original biliary tract tumors**

| Xenograft | Pathological diagnosis of original tumor | Age (years)/Sex | Histologic type | Prognosis (Survival [days]) | Cell line |
|---|---|---|---|---|---|
| 1 | CCC | 70/F | Adeno, mod | Death (402) | NCC-CC1 |
| 2 | CCC | 71/F | Adeno, mod | Death (175) | NCC-CC3-1/-2 |
| 3 | CCC | 59/M | Adeno, mod | Alive (219) | NCC-CC4-1 |
| 4 | Middle BDCa | 58/F | Adeno, mod | Death (299) | NCC-BD1 |
| 5 | Lower BDCa | 77/F | Adeno, mod | Alive (316) | NCC-BD2 |
| 6 | Hilar BDCa | 48/M | Adeno, well | Death (500) | NA |
| 7 | CCC | 54/F | Adeno, mod | Death (181) | NA |
| 8 | CCC | 56/M | Adeno, mod | Death (319) | NA |
| 9 | CCC | 73/M | Adeno, mod | Death (53) | NA |
| 10 | CCC | 54/M | Adeno, mod | Alive (655) | NA |
| 11 | CCC | 45/F | Adeno, mod | Alive (623) | NA |
| 12 | CCC | 72/M | Muc | Alive (647) | NA |
| 13 | Middle BDCa | 54/M | Adeno, mod | Alive (535) | NA |
| 14 | CCC | 69/M | Adeno, mod | Death (174) | NA |
| 15 | Hilar BDCa | 70/M | Adeno, mod | Alive (355) | NA |
| 16 | Middle BDCa | 67/M | Adeno, mod | Alive (450) | NA |
| 17 | CCC | 78/M | Adeno, mod | Alive (299) | NA |
| 18 | Middle BDCa | 66/F | Adeno, mod | Alive (198) | NA |
| 19 | CCC | 66/M | Adeno, mod | Death (168) | NA |

Adeno, adenocarcinoma; CCC, cholangiocellular carcinoma; F, female; hilar BDCa, hilar bile duct carcinoma; lower BDCa, lower third of extrahepatic bile duct carcinoma; M, male; middle BDCa, middle third of extrahepatic bile duct carcinoma; mod, moderately differentiated; muc, mucinous adenocarcinoma; well, well differentiated; NA, not applicable.

**Table 2. Mutation status of *p53* and *KRAS* genes of established novel biliary tract carcinoma cell lines**

| Cell line | *KRAS* (exons 1–2) | | *p53* (exons 5–8) | |
|---|---|---|---|---|
| | Nucleotide change | Amino acid change | Nucleotide change | Amino acid change |
| NCC-BD1 | G37C | G13C | C457T, A463C,G467C | P153S, T155P, R156P |
| NCC-BD2 | WT | WT | Homozygous deletion | No product |
| NCC-CC1 | G35T | G12V | G524A | R175H |
| NCC-CC3-1 | G35A | G12D | WT | WT |
| NCC-CC3-2 | G35A | G12D | WT | WT |
| NCC-CC4-1 | WT | WT | WT | WT |

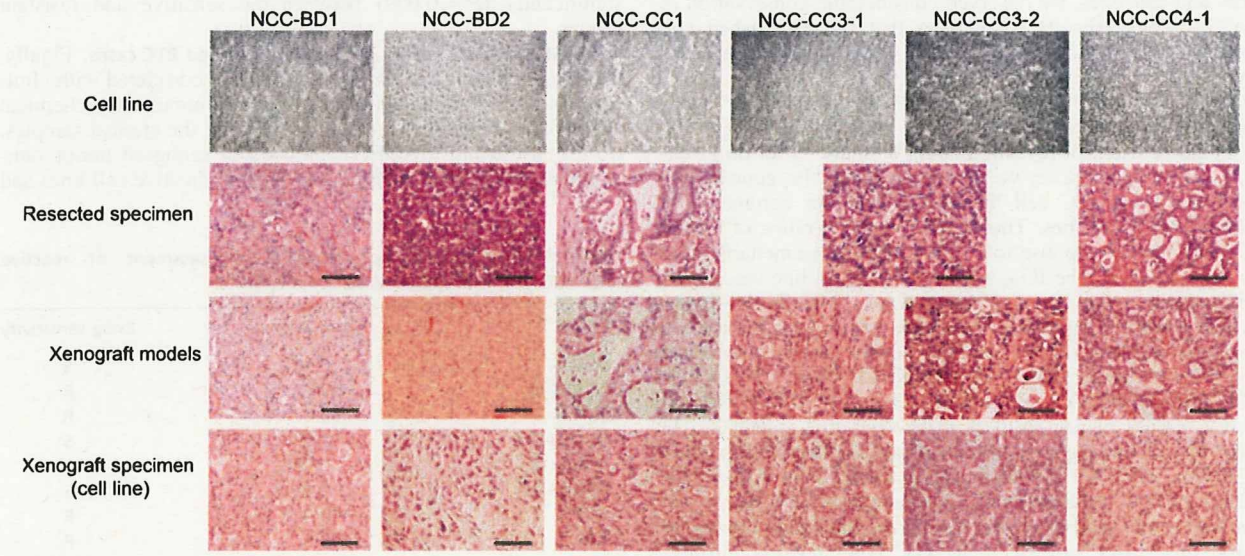


**Fig. 1.** Cell morphology and tumor histology of primary specimen/xenograft of established new biliary tract carcinoma cell lines. *In vitro* cell morphology and tumor histology (H&E staining) of resected primary specimens, xenografts of primary tumor samples and xenografts of cell lines are shown. Scale line = 200 μm.



doi: 10.1111/j.1349-7006.2009.01462.x

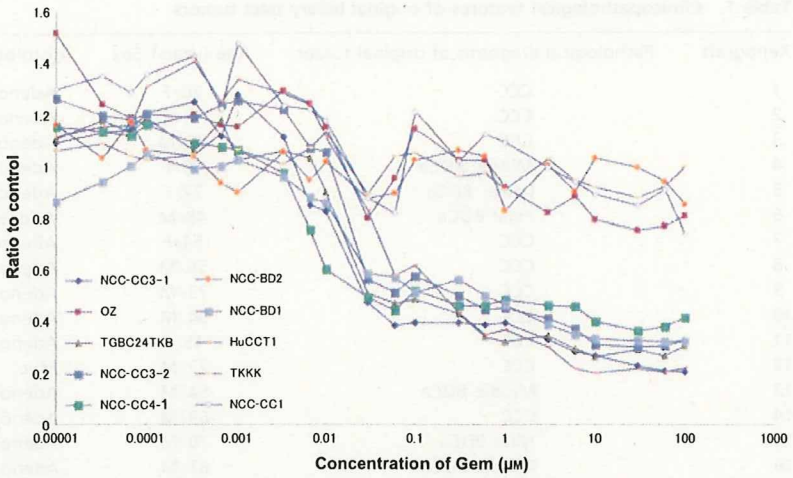


**Fig. 2.** Sensitivity to gemcitabine (Gem) in 10 biliary tract carcinoma cell lines. Ratio of cell proliferation compared to the control (treated with DMSO) at each concentration (μM) of Gem was plotted. Note that 10 cell lines are clearly segregated into two groups (Gem-sensitive and Gem-resistant) with distinct Gem sensitivity.

Nineteen xenograft models (1, 4, 0, 2, and 12 cases of lower, middle, and upper thirds of the extrahepatic bile duct carcinoma, hilar bile duct carcinoma, and intrahepatic cholangiocarcinoma, respectively) were obtained, and six cell lines including two subclones were established through xenograft models (five cell lines) or directly from a surgical specimen (one cell line). The cell lines were designated as NCC-BD1, NCC-BD2, NCC-CC1, NCC-CC3-1, NCC-CC3-2, and NCC-CC4-1, respectively. Four cell lines were derived from intrahepatic BTC and two from extrahepatic BTC (Table 1). Other clinicopathological features of the patients from whom the cell lines were obtained are summarized in Table 1.

Mutation analysis of the *KRAS* and *p53* genes revealed frequent (3/5, 60%) alterations in them. It also confirmed that these new cell lines were of human origin and that two subclones, NCC-CC3-1 and NCC-CC3-2, shared the same *KRAS* mutation (Table 2). The morphology and histology of the established cell lines and primary tumors, and xenografts of primary tumor and cell lines, are shown in Figure 1. As NCC-BD2 cells were unable to form tumors in mice, we used a cell block of this cell line. Comparing the morphological features between primary tumors and cell lines, we observed considerable conservation of tumor histology (Fig. 1), suggesting that the established cell lines could be considered representative of each original primary.

**Classification of 10 BTC cell lines by gemcitabine sensitivity.** We then attempted to evaluate whether these new cell lines could be used for revealing novel biomarkers for drug sensitivity. For this purpose, we first determined the gemcitabine sensitivity of 10 BTC cell lines including four commercially available BTC cell lines. The relative survival ratios of the 10 BTC cell lines in response to various doses of gemcitabine are shown in Figure 2. The $IC_{50}$ value for each cell line was calculated, and the results are summarized in Table 3. Interestingly, as can be seen in Figure 2, on the basis of drug sensitivity, we were able to classify these cell lines into two groups: a gemcitabine-sensitive group that included NCC-BD1, NCC-CC3-1, NCC-CC3-2, NCC-CC4-1, HuCCT1, and TGBC24TKB cells (the $IC_{50}$ values being 0.6, 0.03, 0.06, 0.03, 0.2, and 0.03 μM respectively) and a gemcitabine-resistant group that included NCC-BD2, NCC-CC1, TKKK, and OZ cells, whose $IC_{50}$ values were beyond the range of our measurement (>100 μM). As all of the newly established cell lines were from chemotherapy-naïve tumors, this result suggests that BTC cells possess intrinsic molecular mechanism associated with gemcitabine sensitivity.

**Significant differences in mRNA expression between groups sensitive and resistant to gemcitabine.** To further elucidate the molecular differences between the groups sensitive and resistant to gemcitabine, we investigated the genome-wide mRNA expression in all the cell lines. By comparing the sensitive group with the resistant group, we isolated genes that showed significant differences in expression between the two (Table 4). These included genes associated with cell signaling (*SEC23A*, *RRAS2*, and *BMP8B*) or telomere maintenance (*TERF1*), or genes whose functions were unknown (*NOL10*, *CCDC117*, and *ZSWIM6*). All were candidate biomarkers associated with gemcitabine sensitivity, and among them we focused on MAGEH1 (melanoma antigen family H 1) because: (i) mRNA expression of MAGEH1 in the resistant group was more than five times higher than in the sensitive group; (ii) MAGEH1 is a transmembrane protein that is easily accessible to antibody; and (iii) there was a significant difference in its expression between the two groups ($P = 0.000093$). We then validated the differential expression of MAGEH1 between the two groups by qRT-PCR. As shown in Figure 3, the data for MAGEH1 expression obtained by qRT-PCR, which was normalized with GAPDH expression, was highly correlated with DNA microarray data (coefficient of correlation, 0.847) and also differed significantly ($P = 0.009$) between the sensitive and resistant groups.

**MAGEH1 expression in gemcitabine-treated BTC cases.** Finally, we tested whether MAGEH1 expression is correlated with clinical response to gemcitabine treatment by immunohistochemical analysis of clinical cases. Before analyzing the clinical samples, we tested the anti-MAGEH1 antibody in xenograft tumor samples. Three cell lines (50%) out of the six sensitive cell lines and

**Table 3. Gemcitabine $IC_{50}$ values and assessment of reactive cytotoxicity of biliary tract carcinoma cell lines**

| Cell line | $IC_{50}$ (μM) | Drug sensitivity |
|---|---|---|
| NCC-BD1 | 0.60 | S |
| NCC-BD2 | >100 | R |
| NCC-CC1 | >100 | R |
| NCC-CC3-1 | 0.03 | S |
| NCC-CC3-2 | 0.06 | S |
| NCC-CC4-1 | 0.03 | S |
| TKKK | >100 | R |
| OZ | >100 | R |
| Hucct1 | 0.20 | S |
| TGBC24TKB | 0.03 | S |

R, resistant; S, sensitive.

Table 4. List of genes differentially expressed between gemcitabine sensitive and resistant groups of biliary tract carcinoma cell lines

| Gene symbol | Average expression (R) | Average expression (S) | Ratio (R/S) | *P*-value† | Chromosome locus |
|---|---|---|---|---|---|
| TIMELESS | 1.866235575 | 0.858141402 | 2.174741332 | 1.45E-05 | 12q12-q13 |
| SEC23A | 1.601411675 | 0.796303448 | 2.011057064 | 2.34E-05 | 14q21.1 |
| MAGEH1 | 2.100036325 | 0.397001692 | 5.289741503 | 9.28E-05 | Xp11.21 |
| NOL10 | 1.482213925 | 0.854618707 | 1.734356987 | 0.000201766 | 2p25.1 |
| RRAS2 | 0.221456871 | 1.54467481 | 0.143367956 | 0.000429397 | 11p15.2 |
| BMP8B | 1.7544659 | 0.572194878 | 3.066203432 | 0.000440394 | 1p35-p32 |
| TERF1 | 1.422439425 | 0.778783987 | 1.826487767 | 0.000451224 | 8q13 |
| SEC23A | 1.5599122 | 0.633786226 | 2.461259234 | 0.0004951 | 14q21.1 |
| CCDC117 | 1.71272665 | 0.699035142 | 2.45012954 | 0.000557389 | 22q12.1 |
| C14orf107 | 0.490823853 | 1.299093433 | 0.377820286 | 0.000632072 | 14q22.3 |
| ZSWIM6 | 0.508965063 | 1.33793895 | 0.380409781 | 0.000753833 | 5q12.1 |
| RPL34 | 0.52856332 | 1.102003908 | 0.479638335 | 0.000934328 | 4q25 |

†Obtained using the unpaired *t*-test. R, resistant group; S, sensitive group.

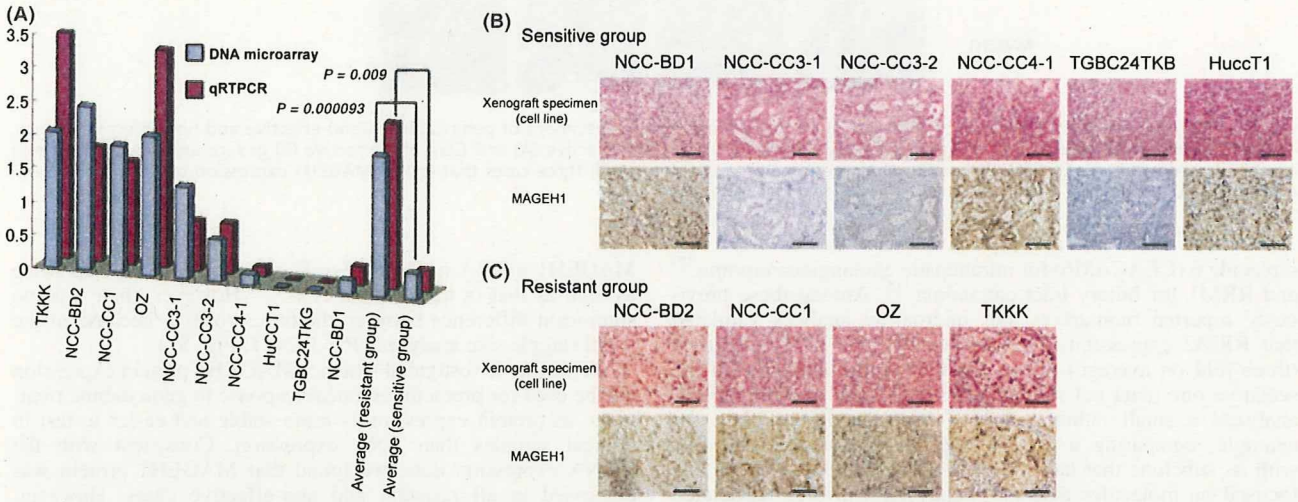


Fig. 3. (A) MAGEH1 mRNA expression in 10 biliary tract carcinoma cell lines. Relative expression of MAGEH1 mRNA compared to GAPDH expression in each cell line was quantified by microarray (blue columns) and quantitative RT-PCR (red columns). MAGEH1 expression was significantly different between gemcitabine (Gem)-sensitive and Gem-resistant groups. (B,C) Immunohistochemical analysis of MAGEH1 protein in xenograft specimens of 10 biliary tract carcinoma cell lines. Tumor histology (H&E staining) of xenograft specimens of cell lines, split into Gem-sensitive (B) and Gem-resistant (C) groups, and MAGEH1 protein expression detected by anti-MAGEH1 antibody in the same area are shown. All three cell lines that lacked MAGEH1 expression belong to the Gem-sensitive group. Scale line = 200 μm.

all four cell lines (100%) in the resistant group were positive for MAGEH1 expression (Fig. 3).

We selected nine recurrent BTC cases treated with gemcitabine alone, which were fully evaluated for drug effects by imaging diagnosis, as described in the "Materials and Methods" section, and whose tumor samples had been sufficiently examined and pathologically diagnosed. After clinical evaluation, we identified five "effective" cases and four "non-effective" cases (Table S2). We examined MAGEH1 protein expression in surgical specimens of the primary tumor in these nine cases. As shown in Figure 4, two (40%) of five "effective" cases were positive, and all four "non-effective" cases (100%) were positive.

## Discussion

Elucidation of the molecular mechanisms determining the biological characteristics of cancer cells is one strategy for improving the clinical outcome of BTC patients, but only a few BTC cell lines serving as potent biological tools and animal models with properties resembling those of human cancer have been established. In this study, we succeeded in establishing six novel BTC cell lines including various subtypes and 19 BTC xenograft models after trying 55 cases. Despite carrying out multiple transplantations, we did not observe any marked discrepancy in cell morphology between the original tumors and the cell lines/xenografts, suggesting that this model could be stable and useful for biological studies. Moreover, we were able to fully combine the corresponding clinical information for patients and pathological archive specimens of primary tumors and xenografts for both primary tumors and cell lines with biological data on the cell lines for both basic and preclinical research. To add more clinically relevant functional data, we examined the gemcitabine sensitivities of these cell lines.

Previously, several predictive markers for the effects of gemcitabine chemotherapy have been reported in various types of tumor, including equilibrative nucleoside transporter-1 (hENT1),[10] ribonucleotide reductase subunit M2 (RRM2),[11] and heat shock protein 27 (HSP27)[12] for pancreatic carcinoma, ribonucleotide reductase subunit M1 (RRM1)[13] for non-small-cell lung cancer (NSCLC), hENT1 for ampulla of Vater carcinoma,[14] carcinoembryonic antigen-related cell adhesion


doi: 10.1111/j.1349-7006.2009.01462.x

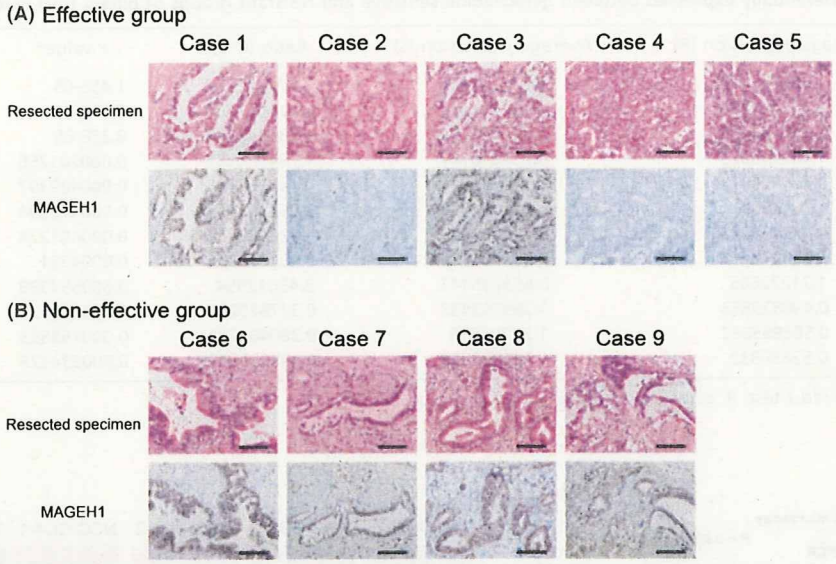


**Fig. 4.** Immunohistochemical analysis of MAGEH1 protein in primary tumor specimens of gemcitabine (Gem)-effective and non-effective groups. Tumor histology (H&E staining) of primary tumor specimens, split into Gem-effective (A) and Gem-non-effective (B) groups and MAGEH1 protein expression detected by anti-MAGEH1 antibody in the same area are shown. All three cases that lacked MAGEH1 expression belong to the Gem-effective group. Scale line = 200 μm.

molecule 6 (CEACAM6) for intrahepatic cholangiocarcinoma,[5] and RRM1 for biliary tract carcinoma.[15] Among these previously reported biomarkers, our microarray analysis validated that RRM2 expression was significantly ($P = 0.03$) increased (three-fold on average) in the resistant group compared to the sensitive one (data not shown). However, most of these studies analyzed a small number of cell lines (maximum two), for example, comparing a gemcitabine-sensitive cancer cell line with its subclone that had acquired gemcitabine resistance, and focused on molecules that are already known to be associated with gemcitabine transport and metabolism. No study has yet tested its efficacy in clinical samples. The present study examined the largest number of BTC cell lines to be detailed in published reports to date, including six novel ones, in relation to clinicopathological information. To discover potential biomarkers in an unbiased way, we examined genome-wide expression profiles using a microarray, identified several biomarker candidates including MAGEH1, and validated its significance in another cohort of clinical BTC cases.

MAGEH1 is a member of the melanoma antigen family (MAGE)[16]. The human MAGE family was originally identified as a tumor-specific antigen,[17] and is now classified into two subtypes (type I and type II).[18] Type I MAGE is completely silenced in normal tissues except male germ cells and placenta, whereas type II MAGE is expressed in both tumors and a fraction of normal tissues. MAGEH1 belongs to the type II MAGE family and is also expressed in normal human tissues.[16] MAGEH1 is expressed in 69% of NSCLC[19] and in 100% of renal cell carcinomas,[20] but no data for BTC have been reported. MAGEH1 associates with the intracellular domain of the p75/NGF receptor[21] and regulates the cell cycle,[19] but its precise role in cancer is largely unknown. In the Gene Expression Omnibus (GEO) database at National Center for Biotechnology Information (NCBI) (http://www.ncbi.nlm.nih.gov/geo/), there is one set of public microarray data showing the association between MAGEH1 expression and gemcitabine resistance in NSCLC cells. Comparison of the gene expression profile of parental Calu3 cell with those of gemcitabine-resistant subclones (Calu3-GemR) revealed that the mean expression of MAGEH1 mRNA in Calu3-GemR clones was more than twice as high as that in the parental cells.[22] However, there was no significant difference between the two, probably because of the small sample size analyzed ($P = 0.2481$; Fig. S1).

We further investigated whether MAGEH1 protein expression can be used for predicting clinical response to gemcitabine treatment, as protein expression is more stable and easier to test in clinical samples than RNA expression. Consistent with the mRNA expression data, we found that MAGEH1 protein was expressed in all resistant and non-effective cases. However, MAGEH1-positive cases also included a portion of sensitive or effective cases, possibly because of post-translational regulation of MAGEH1 protein expression. Significantly, however, MAGEH1-negative cell lines and primary cases were all gemcitabine-sensitive or effective cases, suggesting that MAGEH1 expression could be used as a negative predictor of gemcitabine response. That is, if immunohistochemical staining for MAGEH1 is negative, it is highly likely that a particular case would respond to gemcitabine therapy. Based on its previously reported functions, it remains unclear why MAGEH1 expression would be inversely correlated with gemcitabine response. It could function as a regulator of gemcitabine metabolism or might simply be a surrogate marker of distinct BTC subtypes. Because we analyzed only cases for which the result of gemcitabine treatment had been assessed objectively, it was difficult to collect a large number of retrospective cases. Moreover, we were unable to examine the expression of MAGEH1 RNA in the clinical specimens by RT-PCR because only small amounts of the frozen samples were available. Therefore, further prospective analysis of a larger cohort will be necessary to determine the clinical efficacy of MAGEH1 expression as a predictive biomarker of gemcitabine response.

Recently, a report has indicated that both the amount of stroma and vascularity in the tumor are associated with gemcitabine sensitivity in pancreatic cancer.[23] It was proposed that the hypovascularity and poor vascular architecture of pancreatic ductal carcinomas might impose an additional limitation to therapeutic delivery. Therefore, it was hypothesized that disrupting the stroma of pancreatic tumors might alter the vascular network

and thereby facilitate the delivery of chemotherapeutic agents. Accordingly, we recognized that the tumors in the non-effective group showed a tendency to have more of the stromal component than the tumors in the effective group (Fig. 4). Thus the stromal component would also play an important role in drug resistance of BTC.

In spite of the limited number of cases we examined, our result is consistent with the idea that more complex mechanisms regulate the gemcitabine sensitivity of BTC. In this sense, combination of other biomarker candidates obtained from the present screening or ones discovered through different approaches such as proteomic analysis with MAGEH1 should predict the drug response more accurately. In any event, the present study has shown that our new resource with clinical annotation would be valuable for discovering new biomarkers, and future studies for identifying new therapeutic/diagnostic targets are warranted.

## Acknowledgments

This work was supported by a Grant-in-Aid for Cancer Research from the Ministry of Health, Labor and Welfare of Japan, a Grant-in-Aid for the Third Term Comprehensive 10-Year Strategy for Cancer Control from the Ministry of Health, Labor and Welfare of Japan, and a grant from the program for Promotion of Fundamental Studies in Health Sciences of the National Institute of Biomedical Innovation.

## References

1 Washburn WK, Lewis WD, Jenkins RL. Aggressive surgical resection for cholangiocarcinoma. *Arch Surg* 1995; **130**: 270–6.
2 Kosuge T, Yamamoto J, Shimada K, Yamasaki S, Makuuchi M. Improved surgical results for hilar cholangiocarcinoma with procedures including major hepatic resection. *Ann Surg* 1999; **230**: 663–71.
3 Jang JY, Kim SW, Park DJ *et al.* Actual long-term outcome of extrahepatic bile duct cancer after surgical resection. *Ann Surg* 2005; **241**: 77–84.
4 Sakamoto Y, Kosuge T, Shimada K *et al.* Prognostic factors of surgical resection in middle and distal bile duct cancer: an analysis of 55 patients concerning the significance of ductal and radial margins. *Surgery* 2005; **137**: 396–402.
5 Ieta K, Tanaka F, Utsunomiya T, Kuwano H, Mori M. CEACAM6 gene expression in intrahepatic cholangiocarcinoma. *Br J Cancer* 2006; **95**: 532–40.
6 Khan SA, Thomas HC, Davidson BR, Taylor Robinson SD. Cholangiocarcinoma. *Lancet* 2005; **366**: 1303–14.
7 Thongprasert S. The role of chemotherapy in cholangiocarcinoma. *Ann Oncol* 2005; **16** (Suppl 2): ii93–6.
8 Shi X, Liu S, Kleeff J, Friess H, Buchler MW. Acquired resistance of pancreatic cancer cells towards 5-Fluorouracil and gemcitabine is associated with altered expression of apoptosis-regulating genes. *Oncology* 2002; **62**: 354–62.
9 Eisenhauer EA, Therasse P, Bogaerts J *et al.* New response evaluation criteria in solid tumours: revised RECIST guideline (version 1.1). *Eur J Cancer* 2009; **45**: 228–47.
10 Nakano Y, Tanno S, Koizumi K *et al.* Gemcitabine chemoresistance and molecular markers associated with gemcitabine transport and metabolism in human pancreatic cancer cells. *Br J Cancer* 2007; **96**: 457–63.
11 Duxbury MS, Ito H, Zinner MJ, Ashley SW, Whang EE. RNA interference targeting the M2 subunit of ribonucleotide reductase enhances pancreatic adenocarcinoma chemosensitivity to gemcitabine. *Oncogene* 2004; **23**: 1539–48.
12 Mori Iwamoto S, Kuramitsu Y, Ryozawa S *et al.* Proteomics finding heat shock protein 27 as a biomarker for resistance of pancreatic cancer cells to gemcitabine. *Int J Oncol* 2007; **31**: 1345–50.
13 Rosell R, Danenberg KD, Alberola V *et al.* Ribonucleotide reductase messenger RNA expression and survival in gemcitabine/cisplatin-treated advanced non-small cell lung cancer patients. *Clin Cancer Res* 2004; **10**: 1318–25.
14 Santini D, Perrone G, Vincenzi B *et al.* Human equilibrative nucleoside transporter 1 (hENT1) protein is associated with short survival in resected ampullary cancer. *Ann Oncol* 2008; **19**: 724–8.
15 Ohtaka K, Kohya N, Sato K *et al.* Ribonucleotide reductase subunit M1 is a possible chemoresistance marker to gemcitabine in biliary tract carcinoma. *Oncol Rep* 2008; **20**: 279–86.
16 Chomez P, De Backer O, Bertrand M, De Plaen E, Boon T, Lucas S. An overview of the MAGE gene family with the identification of all human members of the family. *Cancer Res* 2001; **61**: 5544–51.
17 van der Bruggen P, Traversari C, Chomez P *et al.* A gene encoding an antigen recognized by cytolytic T lymphocytes on a human melanoma. *Science* 1991; **254**: 1643–7.
18 Barker PA, Salehi A. The MAGE proteins: emerging roles in cell cycle progression, apoptosis, and neurogenetic disease. *J Neurosci Res* 2002; **67**: 705–12.
19 Tsai JR, Chong IW, Chen YH *et al.* Differential expression profile of MAGE family in non-small-cell lung cancer. *Lung Cancer* 2007; **56**: 185–92.
20 Kramer BF, Schoor O, Kruger T *et al.* MAGED4-expression in renal cell carcinoma and identification of an HLA-A*25-restricted MHC class I ligand from solid tumor tissue. *Cancer Biol Ther* 2005; **4**: 943–8.
21 Tcherpakov M, Bronfman FC, Conticello SG *et al.* The p75 neurotrophin receptor interacts with multiple MAGE proteins. *J Biol Chem* 2002; **277**: 49101–4.
22 Tooker P, Yen WC, Ng SC *et al.* Bexarotene (LGD1069, Targretin), a selective retinoid X receptor agonist, prevents and reverses gemcitabine resistance in NSCLC cells by modulating gene amplification. *Cancer Res* 2007; **67**: 4425–33.
23 Olive KP, Jacobetz MA, Davidson CJ *et al.* Inhibition of Hedgehog signaling enhances delivery of chemotherapy in a mouse model of pancreatic cancer. *Science* 2009; **324**: 1457–61.

## Supporting Information

Additional Supporting Information may be found in the online version of this article:

**Fig. S1.** Mircoarray data of association between MAGEH1 and gemcitabine in non-small lung cancer from NCBI GEO database.

**Table S1.** Primers for mutation analysis of *p53* and *KRAS* genes.

**Table S2.** Clinicopathological feature of 9 patients.

Please note: Wiley-Blackwell are not responsible for the content or functionality of any supporting materials supplied by the authors. Any queries (other than missing material) should be directed to the corresponding author for the article.



doi: 10.1111/j.1349-7006.2009.01462.x

# Intraductal carcinosarcoma with a heterologous mesenchymal component originating in intraductal papillary-mucinous carcinoma (IPMC) of the pancreas with both carcinoma and osteosarcoma cells arising from IPMC cells

Jun Okamura,[1] Shigeki Sekine,[1] Satoshi Nara,[2] Hidenori Ojima,[1] Kazuaki Shimada,[2] Yae Kanai,[1] Nobuyoshi Hiraoka[1]

[1]Pathology Division, National Cancer Center Research Institute, Tokyo, Japan
[2]Division of Hepato-Biliary and Pancreatic Surgery, National Cancer Center Hospital, Tokyo, Japan

**Correspondence to**
Dr Nobuyoshi Hiraoka, Pathology Division, National Cancer Center Research Institute, 5-1-1 Tsukiji, Chuo-ku, Tokyo 104-0045, Japan; nhiraoka@ncc.go.jp

Accepted 9 October 2009

## ABSTRACT

Carcinosarcoma of the pancreas is extremely rare and its histogenesis is still unclear. This is a report on a 64-year-old female patient with an intraductal carcinosarcoma arising from intraductal papillary-mucinous carcinoma (IPMC) in the pancreas tail. The carcinosarcoma grew as a polypoid mass within the main pancreatic duct. Histologically, the tumour consisted of adenocarcinoma covering the luminal surface of the lesion with minimal stromal invasion, and osteosarcoma occupying the stroma. Immunohistochemical and gene mutation analyses revealed that both the carcinomatous and sarcomatous tumour cells of the carcinosarcoma, as well as the IPMC cells, expressed TP53 and had identical mutations in *KRAS* and *TP53* genes, indicating that these two neoplastic components of the carcinosarcoma shared a common tumorigenesis and arose from the IPMC. This is the first report of a carcinosarcoma originating in IPMC. These findings imply that carcinosarcoma with a heterologous mesenchymal component is of ductal origin.

## INTRODUCTION

Carcinosarcoma of the pancreas is a very rare tumour and only several cases have been reported hitherto.[1–6] These cases were diagnosed as carcinosarcoma histopathologically and immunohistochemically on the basis of the presence of both malignant epithelial and malignant mesenchymal components. Only two of the reported cases showed heterologous mesenchymal components.[1 2] The histogenesis of this tumour is still unclear, although there have been several hypotheses that it originates from epithelial cells, mesenchymal cells, undifferentiated precursor cells or stem cells. It has been difficult to assess its histogenesis, because pancreatic carcinosarcoma is extremely rare and is usually advanced at the time of diagnosis.

Here we present the first reported case of pancreatic intraductal carcinosarcoma with a heterologous mesenchymal component (osteosarcoma), which is located in an intraductal papillary-mucinous carcinoma (IPMC). This case is thought to be important for considering the histogenesis of pancreatic carcinosarcoma with a heterologous mesenchymal component.

## CASE REPORT

A 64-year-old Japanese woman who attended our hospital for a health check-up was found by abdominal ultrasonography to have a cystic tumour in the tail of the pancreas. She had no symptoms and all clinical and laboratory data were normal. The serum concentrations of tumour markers were elevated (CA19-9, 87 U/ml; carcinoembryonic antigen (CEA), 2.7 ng/ml). She had been treated for diabetes mellitus for 11 years. Abdominal CT revealed a 2 cm cystic mass in the pancreatic tail (figure 1A). Within the cyst, there were irregular and solid nodules with calculus. The tail of the pancreas had been totally replaced by the tumour. No lymphadenopathy, ascites, liver metastasis or mass in the soft tissues was found. Distal pancreatectomy was performed under a preoperative diagnosis of invasive carcinoma originating in IPMC. The operation was uneventful, and 12 months after surgery, the patient is well without any tumour recurrence or metastasis.

## PATHOLOGICAL AND GENETIC FINDINGS

A grossly elastic, hard, solid, spherical mass measuring 35×21×14 mm was present in the tail of the pancreas. At the cut surface, there was a papillary-to-polypoid projection located in the main and branch pancreatic ducts, which were cystically dilated and filled with clear yellowish mucinous fluid (figure 1B). These intraductal lesions were surrounded by yellowish-grey solid and nodular components of the tumour from the side of the pancreatic tail.

Histologically, the tumour comprised an intraductal neoplasm and a derivative invasive carcinoma (figure 2). The luminal surface of the dilated pancreatic ducts was covered with atypical mucin-secreting columnar epithelial cells showing papillary growth (figure 2A,B), indicating a diagnosis of IPMC. No ovarian-type stroma was evident. It was noteworthy that biphasic histological features were found in the polypoid lesion in the main pancreatic duct, which consisted of papillary proliferation of adenocarcinoma covering the luminal surface of the projecting mass with infrequent and minimal stromal invasion and an osteosarcoma occupying the stroma. The osteosarcoma showed invasive growth, but its extension was limited to the stroma of the IPMC, which was not beyond the duct wall



*J Clin Pathol* 2010;**63**:266–269. doi:10.1136/jcp.2009.071613

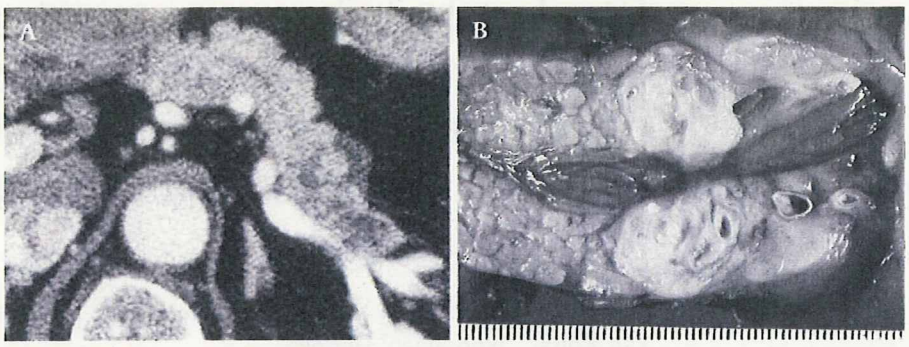


**Figure 1** (A) Abdominal CT image showing a 2 cm cystic mass in the pancreatic tail. (B) Fresh cut view of the body and tail of the pancreas.

(figure 2C–E). The osteosarcoma was characterised by a dense proliferation of malignant spindle-shaped and pleomorphic cells with mononucleated and multinucleated giant cells that had atypical and bizarre nuclei and formed osteoid and bone (figure 2E). Occasional infiltration of osteoclast-like multinucleated giant cells without nuclear atypia was evident. This intraductally proliferating mixed epithelial and mesenchymal tumour was diagnosed as carcinosarcoma, which seemed to have originated in the IPMC. Formation of osteoid and/or bone is rare but possible in cases of undifferentiated carcinoma with osteoclast-like giant cells, although the osteoid and/or bone is a result of reactive stromal metaplasia without any atypia in such cases.[7]

In addition to the intraductal tumour, IPMC cells had infiltrated beyond the duct wall and reached the surrounding stroma, showing a marked desmoplastic reaction at the side of the pancreatic tail bearing the tumour (figure 2B). The infiltrating cancer cells proliferated with poorly formed glands and solid to nested growth, indicating poorly differentiated adenocarcinoma. The infiltrating adenocarcinoma formed a nodular mass measuring 25×21×14 mm, although the invasive adenocarcinoma was not connected to the intraductal carcinosarcoma.

Immunohistochemical examination revealed expression of cytokeratins (AE1/AE3 and CK7) and vimentin, which

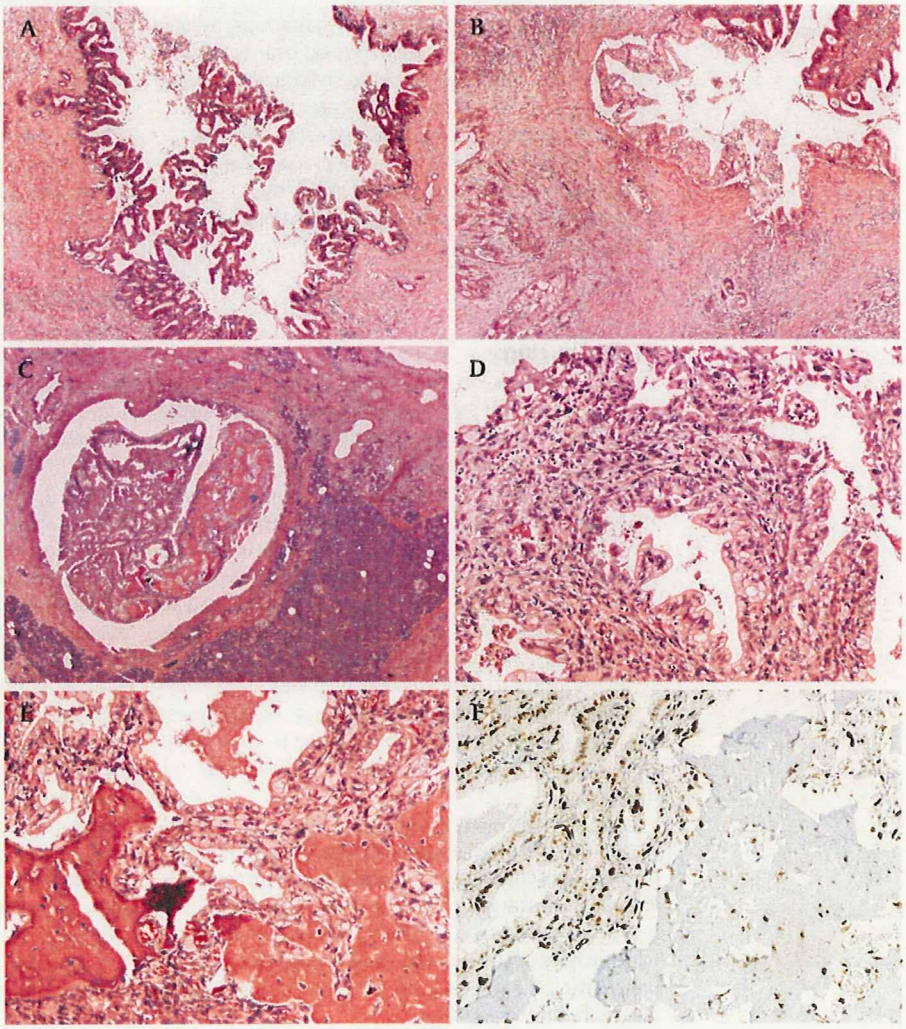


**Figure 2** (A, B) Histopathological features of intraductal papillary-mucinous carcinoma (IPMC) (A) and invasive adenocarcinoma arising from IPMC (B). (C–E) Histopathological features of intraductal carcinosarcoma originating in IPMC. (C) A very-low-power view of the polypoid lesion in the main pancreatic duct. (D, E) Mid-power view of the polypoid lesion. (F) Immunohistochemical expression of TP53 in intraductal carcinosarcoma originating in IPMC.

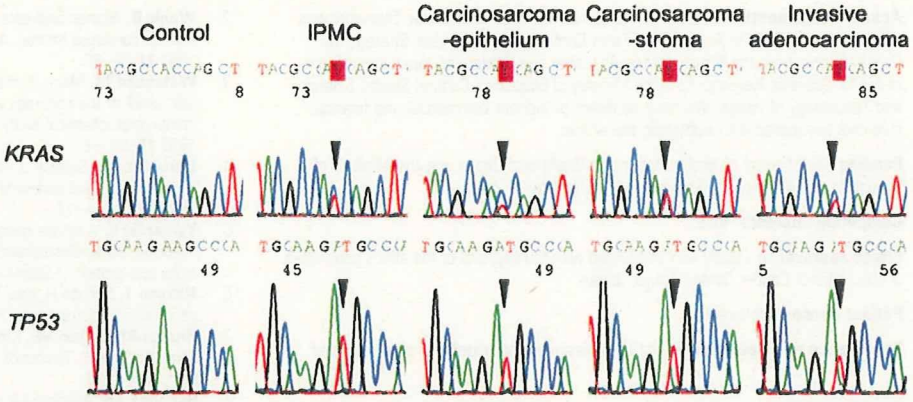


**Figure 3** Mutations of *KRAS* and *TP53* genes in each tumour component. All four tumour components examined (epithelial and mesenchymal tumour cells in the carcinosarcoma, intraductal papillary-mucinous carcinoma (IPMC) cells and invasive adenocarcinoma cells), harboured identical *KRAS* and *TP53* mutations. The sequences were read with reverse primers. Triangles indicate locations of point mutations.

confirmed the epithelial and mesenchymal components of tumour cells detected histologically. TP53 was expressed in the nuclei of most of the intraductal and invasive epithelial tumour cells as well as the mesenchymal tumour cells (figure 2F). CD68 antigen was expressed in some of the multinucleated giant cells without nuclear atypia. These CD68-positive osteolclast-like giant cells did not express TP53.

Four distinct tumour components (epithelial and mesenchymal tumour cells in the carcinosarcoma, IPMC cells and invasive adenocarcinoma cells) were separately laser-microdissected and analysed for *KRAS* and *TP53* mutations. DNA samples extracted from the microdissected tissues were subjected to PCR with a pair of specific primers to amplify exon 1 of *KRAS* or exon 4 of *TP53*, and isolated PCR products were sequenced bidirectionally. The analysis revealed identical *KRAS* (G35A mutation in exon 1) and *TP53* (T337A mutation in exon 4) mutations in all four tumour components examined (figure 3). Non-neoplastic pancreatic parenchyma adjacent to the tumour exhibited wild-type sequences, confirming the somatic nature of the mutations.

## DISCUSSION

Carcinosarcoma is a biphasic tumour consisting of an intimate admixture of malignant epithelial and mesenchymal components identifiable on the basis of their morphological, immunohistochemical and sometimes ultrastructural features. Nine cases of carcinosarcoma of the pancreas have been reported,[1–6] including two with heterologous mesenchymal components; one of the latter cases exhibited leiomyosarcoma, chondrosarcoma and rhabdomyosarcoma,[1] and the other showed malignant nerve sheath tumour as heterologous mesenchymal components.[2] No case of either carcinosarcoma arose from intraductal papillary-mucinous neoplasm (IPMN) and all were found at an advanced stage, with an average tumour diameter of 9.6 cm (range 2.5–19 cm).

To our knowledge, the present case of carcinosarcoma with a heterologous mesenchymal component originating in IPMN is the first of its kind to have been reported. Immunohistochemical and gene mutation analyses revealed that both the carcinomatous and sarcomatous tumour cells in the carcinosarcoma as well as the IPMC cells expressed TP53 and had common mutations in *KRAS* and *TP53* genes, indicating that these two neoplastic components of the carcinosarcoma had a common origin, IPMC. This case provides new findings supporting the hypothesis that carcinosarcoma with a heterologous mesenchymal component is of ductal origin and arises from IPMN.

The histogenesis of carcinosarcoma is still controversial, but the previously proposed hypotheses have now been combined as the following: (1) it is a combination tumour in which carcinomatous and sarcomatous elements arise from a multipotential stem cell; (2) it is a collision tumour in which two independent neoplasia, carcinoma and sarcoma, develop; (3) it is a carcinoma showing metaplastic changes to sarcoma components. The definition of carcinosarcoma in the WHO histological classification differs according to the organ in which the tumour develops. A mixed epithelial and mesenchymal tumour with heterologous mesenchymal components is defined as carcinosarcoma in the histological classification of tumours of many organs, including the colon and rectum, gallbladder and extrahepatic bile ducts, and lung.[8] In contrast, a mixed epithelial and mesenchymal tumour, regardless of the presence of heterologous mesenchymal components, is defined as carcinosarcoma in the histological classification of tumours of the breast and female genital tract. It is thought that most, but not all, of the mesenchymal components in carcinosarcoma of the female genital tract arise from the carcinoma through metaplastic change and that the small population of the carcinosarcoma left is formed by collision of carcinoma and sarcoma.[9] The present case suggests that carcinosarcoma of the pancreas arises from a carcinoma with metaplastic changes, although the WHO histological classification of pancreatic tumours includes no specific category for carcinosarcoma.[8] According to the previous report,[2] a sarcomatous component is speculated to arise from ovarian-type stroma characteristic of mucinous cystic neoplasm. In such a case, carcinosarcoma should be formed as a collision tumour.

In summary, we have presented a case of pancreatic intraductal carcinosarcoma originating in IPMC. Our morphological, immunohistochemical and genetic findings suggest that the carcinosarcoma with a heterologous mesenchymal component was ductal in origin.

### Take-home messages

- Carcinosarcoma of the pancreas is extremely rare and its histogenesis is still unclear.
- We describe an intraductal carcinosarcoma arising from intraductal papillary-mucinous carcinoma (IPMC) in the pancreas tail.
- Both the epithelial component (adenocarcinoma) and heterologous mesenchymal component (osteosarcoma) of the carcinosarcoma, as well as the IPMC, expressed TP53 and had identical mutations in *KRAS* and *TP53* genes, indicating that these two neoplastic components of the carcinosarcoma shared a common tumorigenesis and arose from the IPMC. These findings imply that carcinosarcoma with a heterologous mesenchymal component is of ductal origin.



*J Clin Pathol* 2010;**63**:266–269. doi:10.1136/jcp.2009.071613

**Acknowledgements** We thank Ms Rie Itoh for technical assistance. This work was supported by a Grant-in-Aid for Third Term Comprehensive 10-year Strategy for Cancer Control from the Ministry of Health, Labor and Welfare of Japan and a Grant-in-Aid for Scientific Research from the Ministry of Education, Culture, Sports, Science and Technology of Japan. We have no direct or indirect commercial and financial incentive associated with publishing the article.

**Funding** The Ministry of Health, Labor and Welfare of Japan and the Ministry of Education, Culture, Sports, Science and Technology of Japan.

**Competing interests** None.

**Ethics approval** This study was conducted with the approval of the ethics committee of the National Cancer Center, Tokyo, Japan.

**Patient consent** Obtained.

**Provenance and peer review** Not commissioned; not externally peer reviewed.

## REFERENCES

1. **Millis JM,** Chang B, Zinner MJ, *et al*. Malignant mixed tumor (carcinosarcoma) of the pancreas: A case report supporting organ-induced differentiation of malignancy. *Surgery* 1994;**115**:132–7.
2. **Wenig B,** Albores-Saavedra J, Buetow P, *et al*. Pancreatic mucinous cystic neoplasm with sarcomatous stroma: A report of three cases. *Am J Surg Pathol* 1997;**21**:70–80.
3. **Watanabe M,** Miura H, Inoue H, *et al*. Mixed osteoclastic/pleomorphic-type giant cell tumor of the pancreas with ductal adenocarcinoma: Histochemical and immunohistochemical study with review of the literature. *Pancreas* 1997;**15**:201–8.
4. **Darvishian F,** Sullivan J, Teichberg S, *et al*. Carcinosarcoma of the pancreas: A case report and review of the literature. *Arch Pathol Lab Med* 2002;**126**:1114–17.
5. **Yamazaki K.** A unique pancreatic ductal adenocarcinoma with carcinosarcomatous histology, immunohistochemical distribution of hCG-beta, and the elevation of serum alpha-feto-protein. *J Submicrosc Cytol Pathol* 2003;**35**:343–9.
6. **Nakano T,** Sonobe H, Usui T, *et al*. Immunohistochemistry and K-ras sequence of pancreatic carcinosarcoma. *Pathol Int* 2008;**58**:672–7.
7. **Hruban RH,** Pitman MB, Klimstra DS. eds. *AFIP Atlas of the Tumor Pathology Fourth Series Fascicle 6: Tumors of the Pancreas*. Washington, DC: American Registry of Pathology, 2007.
8. **Hamilton SR,** Aaltonen LA, eds. *Pathology and genetics. Tumours of the digestive system. World Health Organization Classification of Tumours*. Lyon, France: IARC Press, 2000.
9. **McCluggage WG.** Malignant biphasic uterine tumors: carcinosarcomas or metaplastic carcinomas? *J Clin Pathol* 2002;**55**:321–5.

Cancer Science
The official journal of the Japanese Cancer Association JCA

# Fibroblast growth factor receptor 3 mutation in voided urine is a useful diagnostic marker and significant indicator of tumor recurrence in non-muscle invasive bladder cancer

Makito Miyake,[1,8] Kokichi Sugano,[1,9] Hitomi Sugino,[1] Kazuho Imai,[1] Eri Matsumoto,[1] Koshi Maeda,[2] Shinich Fukuzono,[2] Hiroki Ichikawa,[3] Kiyotaka Kawashima,[3] Kaoru Hirabayashi,[4] Tetsuro Kodama,[5] Hiroyuki Fujimoto,[6] Tadao Kakizoe,[6] Yae Kanai,[7] Kiyohide Fujimoto[8] and Yoshihiko Hirao[8]

[1]Oncogene Research Unit/Cancer Prevention Unit, Tochigi Cancer Center Research Institute, 4-9-13 Yonan, Utsunomiya; [2]Hitachi High-Technologies Corporation, Hitachinaka, Ibaraki; [3]Department of Urology, [4]Department of Clinical Laboratory, [5]Director, Tochigi Cancer Center Hospital, Utsunomiya, Tochigi; [6]Department of Urology, National Cancer Center Hospital, [7]Pathology Division, National Cancer Center Research Institute, Tokyo; [8]Department of Urology, Nara Medical University, Kashihara, Nara, Japan

(Received May 06, 2009/Revised August 17, 2009/Accepted August 23, 2009/Online publication October 14, 2009)

**The fibroblast growth factor receptor (FGFR)-3 gene encodes a receptor tyrosine kinase that is frequently mutated in non-muscle invasive bladder cancer (NMIBC). A sensitive and quantitative assay using peptide nucleic acid-mediated real-time PCR was developed for detecting *FGFR3* mutations in the urine samples and evaluated as a molecular marker for detecting intravesical recurrence of NMIBC in patients undergoing transurethral resection of bladder tumor. *FGFR3* mutation was examined in tumor tissues and serially taken pre- and postoperative urine sediments in 45 NMIBC patients with a median follow up of 32 months. *FGFR3* mutations were detected in 53.3% (24/45) of primary tumor tissues, among which intravesical recurrence developed in 37.5% (9/24) of cases. *FGFR3* mutation in the primary tumor was not a significant prognostic indicator for recurrence, while the proportion of *FGFR3* mutation (i.e. tumor cellularity was ≥11%) in the preoperative urine sediments was a significant indicator for recurrence in patients with *FGFR3* mutations in the primary tumors. *FGFR3* mutations were detected in 78% (7/9) of postoperative urine samples from recurrent cases with *FGFR3* mutations in the tumor, while no mutations were detected in the urine of 15 non-recurrent cases. Urine cytology was negative in all cases with *FGFR3* mutations in the primary tumors, while the sensitivity of cytological examination was as high as 56% (5/9) in cases showing wild-type *FGFR3* in the primary tumors. Urine *FGFR3* mutation assay and cytological examination may be available in the future as complementary diagnostic modalities in postoperative management of NMIBC. (*Cancer Sci* 2010; 101: 250–258)**

Urothelial carcinoma (UC) is a histological subtype accounting for more than 90% of all bladder cancers, and there are 357 000 new cases every year worldwide.[1] Bladder UCs are generally divided into two groups for clinical management, depending on the pathological stage. Most of the newly diagnosed UCs are non-muscle invasive bladder cancer (NMIBC; i.e., pTa or pT1), and the initial treatment is transurethral resection of bladder tumor (TURBT). After the initial TURBT, the patients undergo intensive surveillance by cystoscopic examination at regular intervals; usually every 3 months, because up to 70% of these patients will experience intravesical recurrence, and 10–30% of the lesions will progress to life-threatening muscle-invasive disease (≥pT2).[2] Cystoscopy is an inconvenient, invasive, and expensive diagnostic modality, but currently it is the gold standard for detecting intravesical recurrence in the postoperative follow up. Although urine bound diagnostic tests including urinary cytology, nuclear matrix protein (NMP)22, and bladder tumour antigen (BTA) tests are used in the management after TURBT or bladder cancer screening, their usefullness is limited due to their poor sensitivity or specificity.[3] In previous reports, various molecular markers detectable in urine have been considered as a useful and non-invasive clinical assay improving the sensitivity of conventional tests.[4–10] In urine-based detection assays, contamination with normal urothelium or leucocytes can mask the signals of targeted somatic mutations.[11]

Fibroblast growth factor receptor (FGFR)-3 belongs to a family of structurally related tyrosine kinase receptors (FGFR1–4), and plays important roles in many biological processes including embryogenesis, proliferation, differentiation, and angiogenesis.[12] Recent reports have demonstrated that constitutively activated *FGFR3* mutations exist in more than 50% of primary bladder UC.[13] *FGFR3* mutations are especially prevalent in the low-grade papillary tumors (pTa/G1), but they are infrequent in high-grade or high-stage UC.[13,14] *FGFR3* mutation in urine sediments may be a suitable biomarker for detection of low-grade and low-stage UC. Previous studies revealed that mutation of *FGFR3* in the voided urine can be detected at high sensitivity in patients with *FGFR3*-mutated bladder UC.[15–17] However, there is no report validating the feasibility and usefulness of detecting *FGFR3* mutation in the voided urine samples by serial determinations during follow up after TURBT. Recently, we have reported an assay protocol for detecting *FGFR3* mutations in bladder tumor tissues and urine sediments by peptide nucleic acid (PNA)-mediated real-time PCR clamping assay.[17] In PNA-mediated PCR clamping, PNA is designed to anneal to a wild-type DNA sequence and inhibits the annealing of PCR primer to the wild-type alleles, resulting in preferential amplification of the mutated alleles. With 50 ng of genomic DNA as a template, this method allows sensitive and quantitative detection of the *FGFR3* mutations in mutational hotspots in exons 7, 10, and 15 in bladder cancer. In the present study, we modified the protocol of the PNA-mediated PCR clamping assay to achieve quantitative detection of the *FGFR3* mutations present in the urine samples at a concentration of 1% in only 1 ng of genomic DNA available as a template for PCR. With this the revised protocol, we assessed the usefulness of *FGFR3* mutations as a

[9]To whom correspondence should be addressed.
E-mail: ksugano@tcc.pref.tochigi.lg.jp



doi: 10.1111/j.1349-7006.2009.01334.x

diagnostic modality in the voided urine samples for the postoperative management of NMIBC. This is considered the first report addressing the significance of *FGFR3* mutations in preoperative urine sediments as a novel indicator predicting the risk of intravesical recurrence of NMIBC.

## Materials and Methods

**Subjects and collection of the tumor tissues and voided urine samples after the initial TURBT.** The patients undergoing TURBT from April 2002 through March 2005 at the Departments of Urology at Tochigi Cancer Center Hospital and Nara Medical University Hospital were enrolled in this study. All participants had received study information and signed a written informed consent form. The voided urine samples before the initial TURBT were taken from the patients. The resected tumors were examined histologically and staged and graded according to the 2002 TNM classification and the 1973 World Health Organization (WHO) classification systems, respectively.[18,19] A total of 45 subjects with NMIBC were eligible for the study and were followed up until the histological diagnosis of tumor recurrence or up to 3 years postoperatively by routine cystoscopy and urine cytological examination. The median follow-up period was 32 months (range 4–36 months). The patients were monitored by routine cystoscopy and urine cytology at 1, 3, 6, 9, 12, 15, 18, 21, 24, 30, and 36 months after the initial TURBT. Intravesical recurrence was confirmed by histological diagnosis of tumor tissues obtained during TURBT for recurrence. The voided urine samples were divided and subjected to urine cytology and DNA extraction for gene testing. The urine samples were stored at −20°C until DNA extraction.

**DNA extraction and measurement of DNA concentration.** DNA extraction from the tumor tissues and peripheral blood lymphocytes (PBL) was carried out as described previously.[6] DNA extraction from the urine samples was carried out with the QIAamp DNA Blood Mini Kit (Qiagen, Valencia, CA, USA) according to the manufacturer's instructions. Briefly, the urine sample in a 50-mL tube was centrifuged at 180*g* for 5 min. The cell pellet was digested by Qiagen protease and subjected to DNA extraction by column centrifugation. In the final step, DNA was eluted from the column in 150 μL of the elution buffer. The genomic DNA concentration was determined by ultraviolet measurement using an ND-1000 spectrophotometer (NanoDrop Technologies, Wilmington, DE, USA). For analysis of samples with DNA concentrations less than 50 ng/μL, DNA concentration was quantified by real-time PCR using LightCycler (Roche Diagnostics, Mannheim, Germany). Quantification was carried out with the same primer pairs used for PNA-mediated real-time PCR clamping for amplification of *FGFR3* exon 7.[17] Serially diluted assay standards were prepared by adjusting the genomic DNA concentrations to 100, 10, 1, and 0.1 ng/μL. DNA samples and assay standards were subjected to real-time PCR in a 20-μL reaction volume containing genomic DNA, 10 picomole of each primer, and 10 μL of QuantiTect PCR master mix (Qiagen) containing SYBR Green I dye. The conditions of real-time PCR are described in Table 1. DNA concentration was calculated from the crossing points (CP) of the assay standards and samples according to the fit points method on LightCycler Data Analysis software version 3.5 (Roche Diagnostics corporation).

**PNA-mediated pre-main amplifier method for the low-copy number DNA template.** Previously, we reported a PNA-mediated real-time PCR clamping assay for detection of *FGFR3* mutations.[17] This method enabled sensitive and reproducible detection of *FGFR3* mutations in cases where 50 ng of genomic DNA were available as the template for PCR. In the PNA-mediated PCR-clamping, the chance of nucleotide misincorporation to the PNA binding sequence increases in reverse correlation with the amount of template DNA. When the amount of template DNA was 1 ng in genomic DNA (equivalent to 300 copies), mutations were hardly distinguishable from those caused by misincorporation of dNTPs. To overcome this pitfall, we modified the assay protocol to detect *FGFR3* mutations at a concentration of 1% (three copies) in 1 ng (300 copies) of the template genomic DNA. We called the newly established method as PNA-mediated pre-main amplifier (PPA), which consisted of two steps of amplification (Fig. 1). Low-copy number DNA template was amplified by the pre-amplifier step and then set on the main amplifier to perform the PNA-mediated real-time PCR clamping. Pre-amplification was carried out in a PCR tube using DNA Engine Dyad Thermal Cycler (MJ Research, Watertown, MA, USA) in 20-μL aliquots consisting of 1 ng of genomic DNA, 10 μL of QuantiTect PCR master mix, and 10 picomole of each primer. The sequences of primer pairs were as reported previously.[17] Conditions of the thermal cycling in the pre-amplifier step were as follows: denaturing at 95°C for 15 min, amplification of seven cycles consisting of heat denaturation at 94°C for 15 s, annealing at 64°C (exon 7), 58°C (exon 10), and 60°C (exon 15) for 20 s, and extension at 72°C for 20 s. After final cooling to 4°C, 5 μL of the solution containing 2.5 μL of QuantiTect PCR master mix and 2.5 μL of PNA solution were added and mixed by gentle pipetting. The sequences of PNA and the final concentrations are listed in Table 1. Of 25 μL of the mixed solution, 20 μL was transferred to a capillary tube for the LightCycler and set on the main amplifier performing the real-time PCR (Table 1). CP of PPA were determined by the fit points method.

**Detection of *FGFR3* mutations in the tumor tissues and urine samples.** The assay standards for mutation analysis of each exon were prepared as described previously.[17] In the clinical

**Table 1. Sequences of PCR primers and peptide nucleic acid (PNA), and PCR conditions**

| Real-time PCR | Sequence of primers and PNA | PNA concentration (μM) | Cycle no. | PNA binding step (°C) | Annealing step (°C) |
|---|---|---|---|---|---|
| DNA quantification | 5′-TGA GCG TCA TCT GCC CCC ACA GAG-3′ (sense)<br>5′-GGG CCC ACC TTG CTG CCA TTC A-3′ (antisense) | – | 45 | – | 64 |
| Main amplifier for exon 7 | 5′-TGA GCG TCA TCT GCC CCC ACA GAG-3′ (sense)<br>5′-GGG CCC ACC TTG CTG CCA TTC A-3′ (antisense)<br>H2N-AGC GCT CCC CGC ACC-N2H (PNA) | 0.4 | 45 | 72 | 64 |
| Main amplifier for exon 10 | 5′-CCA GGC CTC AAC GCC CAT GTC TTT-3′ (sense)<br>5′-ACC CCG TAG CTG AGG ATG CCT GCA-3′ (antisense)<br>H2N-CAT ACA CAC TGC CCG C-N2H | 1 | 45 | 67 | 58 |
| Main amplifier for exon 15 | 5′-GCA ATG TGC TGG TGA CCG AG-3′ (sense)<br>5′-CGG GCT CAC GTT GGT CGT CT-3′ (antisense)<br>H2N-GGT CGT CTT CTT GTA GT-N2H | 2 | 45 | 70 | 60 |

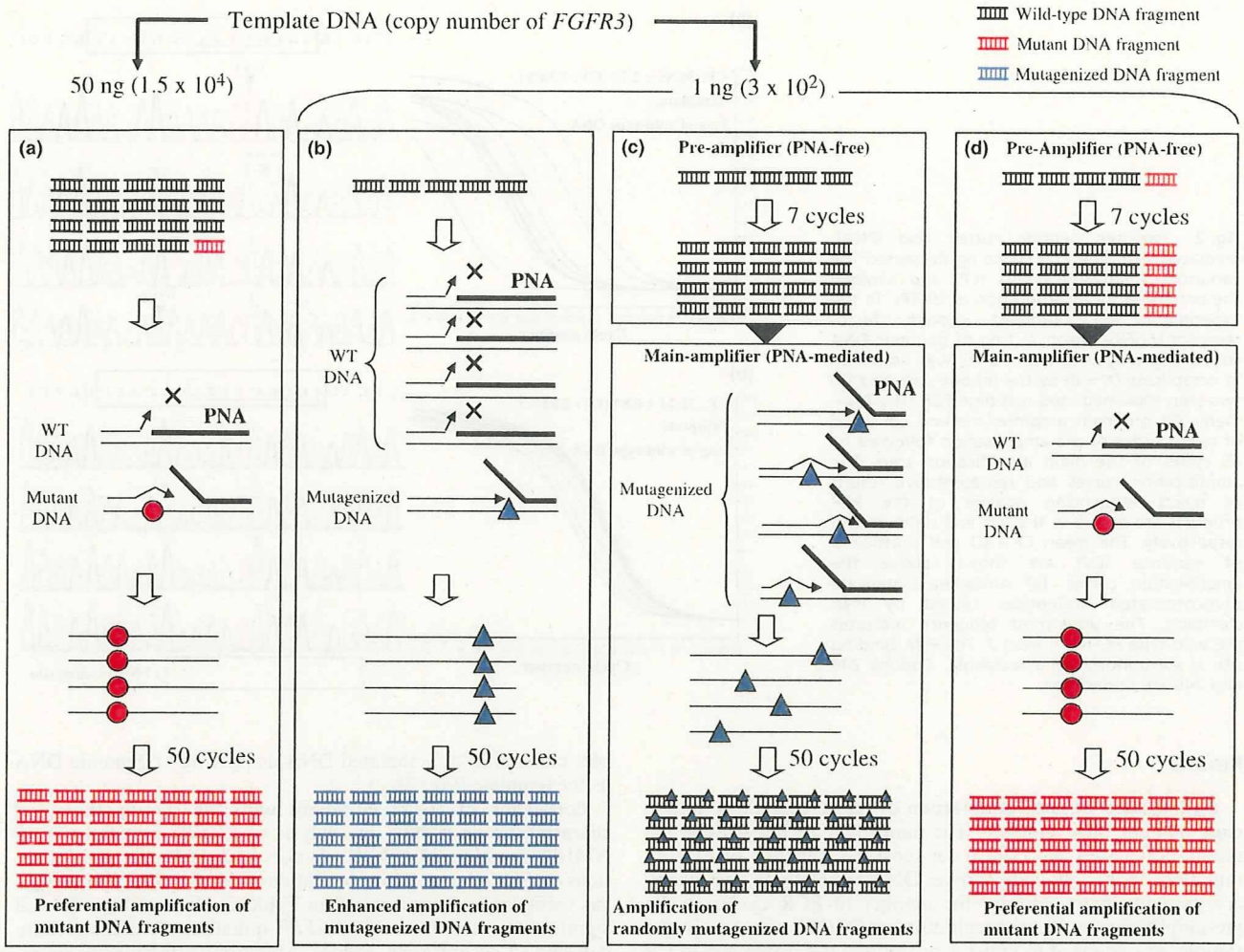


**Fig. 1.** Schematic diagram of the one-step and two-step peptide nucleic acid (PNA)-mediated PCR clamping. The feasibility of PNA-mediated PCR clamping was highly influenced by the amount of the template DNA. (a) Fifty nanograms of genomic DNA containing a low proportion of mutated DNA was used as a template. PNA-mediated PCR enabled preferential amplification of the mutated DNA, leading to enrichment of the mutated DNA fragments. The red circle indicates a mutated DNA sequence. (b) One nanogram of genomic DNA containing only wild-type DNA was used as the template. Misincorporation of dNTPs occurred in the sequences of the PNA-binding site, due to a failure in DNA synthesis brought about by DNA polymerase. When the nucleotide misincorporation (blue triangle) occurred in the early cycles of PNA-mediated PCR, a mutagenized sequence was subjected to subsequent amplification. (c) One nanogram of the template DNA containing only wild-type DNA was used for the PNA-free pre-amplifier step prior to the PNA-mediated main-amplifier. Seven PCR cycles of the pre-amplifier step generated sufficient copies of fibroblast growth factor receptor (*FGFR*)-3 DNA fragments, which were used as the template for the main-amplifier. The PNA-mediated reaction produced a randomly mutagenized DNA sequence that could slip from PNA clamping. However, all of these mutagenized fragments resulted in dispersion of mutagenesis signals and were scarcely detectable in the direct sequencing analysis. (d) One nanogram of genomic DNA with a low proportion of mutant DNA was used as the template. The PNA-free pre-amplifier increased the copy numbers of the *FGFR3* molecules as a whole, leading to a successful preferential amplification of the mutated DNA fragments in the main-amplifier. The black, red, and blue fragments indicate the wild-type, mutated, and mutagenized DNA fragments, respectively.

samples with DNA concentrations of ≥50 ng/μL, mutation analyses were carried out according to the one-step assay using 50 ng of genomic DNA as the template.[17] In the samples with DNA concentrations ranging from 0.125 to 50 ng/μL, a modified protocol was adapted using 1 ng of genomic DNA as the template. In each run, we defined CP of the assay standard corresponding to 1% tumor cellularity as the minimal detectable dose for *FGFR3* mutations. Accordingly, a sample showing CP less than that of the 1% assay standard was considered mutation positive and subjected to direct sequencing to identify the mutational types.[17] The tumor cellularities of the mutation-positive samples were determined by a regression analysis using a standard curve obtained from 100, 10, and 1% assay standards. The samples with DNA concentrations less than 0.125 ng/μL were regarded as unavailable samples unless they could be enriched in DNA concentration.

**Statistical analysis.** Statistical analyses and drawing figures were done using PRISM software version 4.00 (GraphPad Software, Inc., San Diego, CA, USA). Student's *t*-test, Chi-square test, and Fisher's exact test were used to analyze the correlations between the clinicopathological variables and *FGFR3* mutational status in the primary tumors. Recurrence-free survival curves were plotted according to the Kaplan–Meier method, and the log-rank test was applied for statistical significance. A receiver operating characteristic (ROC) curve was used to define the optimal cut-off value of tumor cellularity in the urine sediments. The non-parametric variables were analyzed by the Mann–Whitney *U*-test. A *P*-value of $<0.05$ was considered significant.



doi: 10.1111/j.1349-7006.2009.01334.x

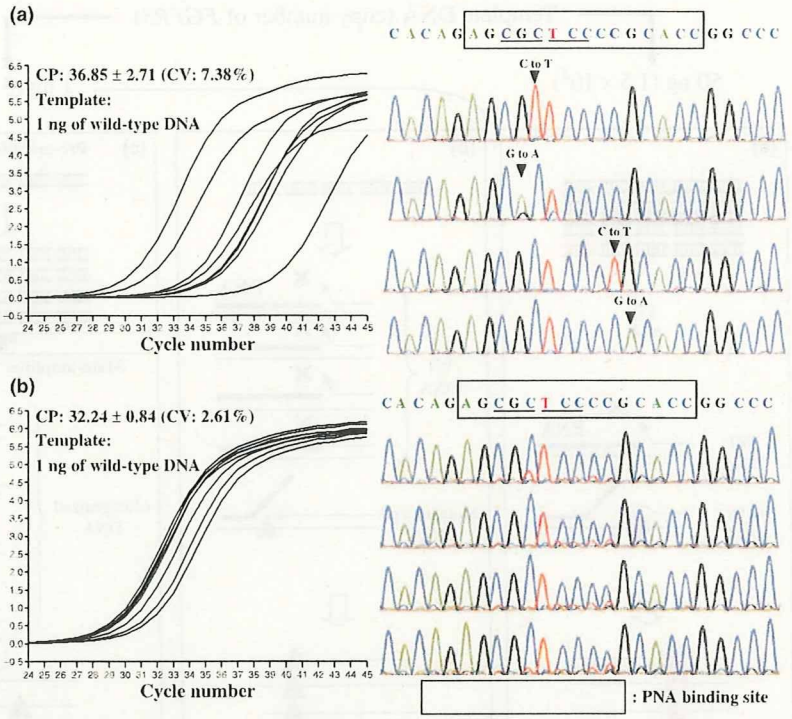


**Fig. 2.** Two-step peptide nucleic acid (PNA)-mediated real-time PCR clamping decreased the variance of crossing points (CP) and avoided the enhanced misincorporation of dNTPs. In the experiment for fibroblast growth factor receptor (*FGFR*)-3 exon 7, 1 ng of genomic DNA containing only wild-type *FGFR3* was amplified in octaplicate ($n$ = 8) by the (a) one-step and (b) two-step PNA-mediated real-time PCR. The PNA-mediated pre-main amplifier method consisted of seven cycles of pre-amplification followed by 45 cycles of the main amplification step. The amplification curves and representative results of direct sequencing analysis of the PCR products are shown in the left and right panels, respectively. The mean CP ± SD and coefficient of variance (CV) are shown above the amplification curves. (a) Arrowheads indicate disincorporated nucleotides caused by PNA clamping. The uppermost sequence indicates the wild-type *FGFR3* in exon 7. The PNA binding site is surrounded by a rectangle. Codons 248 and 249 are underlined.

## Results

**Optimization of PPA for detection of *FGFR3* mutations in low-copy number DNA template.** The number of PCR cycles in the pre-amplifier step was critical for sensitive detection of *FGFR3* mutations in the low-copy number DNA template. In a preliminary experiment to optimize the number of PCR cycles in the pre-amplifier step, the concentration of *FGFR3* mutation in the sample was adjusted to either 1 or 0% and the difference in CP was maximal when seven cycles of PCR were used in the pre-amplification step ($P$ = 0.001). In this condition, we compared the coefficients of variation (CV) between the one-step and two-step assays using 1 ng of wild-type genomic DNA as the template (Fig. 2a,b left). The assay CV of CP in the PPA method was much smaller than that of the one-step assay (2.61 vs 7.38%, respectively). The sequencing analysis of the amplified DNA fragments in the one-step assay revealed point mutations caused by nucleotide misincorporation virtually in all samples (Fig. 2a right), whereas those amplified by the PPA assay showed no recognizable mutations except for a slight increase in the background signals. These results indicated that the PPA method circumvented the chance of a nucleotide misincorporation and minimized the CV of the CP for wild-type DNA or 0% standard (Fig. 2b right). In this condition, the assay standards with 100, 10, and 1% mutations in exon 7 of *FGFR3* and 0% (wild type) were amplified by the PPA method using 1 ng of DNA template, and the results were compared with those of the one-step assays. The CPs of the assay standards were statistically significant between each other (Fig. 3a) and direct sequencing analysis of the 1% standard revealed that all of eight samples showed S249C mutation (TCC → TGC) in exon 7. These results demonstrated that the mutations were reliably detected in the samples containing ≥1% mutated DNA using only 1 ng of DNA template, and that the PPA method overcame the limitation of our prior study.

In analysis of exons 10 and 15, seven amplification cycles in the pre-amplifier step were used to detect mutations in the samples containing ≥1% mutated DNA using 1 ng of genomic DNA as the template (Fig. 3b,c).

**Correlation of *FGFR3* mutations with the clinicopathological characteristics in NMIBC.** In analysis of *FGFR3* mutations in 45 NMIBC samples, 24 (53.3%) tumors harbored activating mutations of *FGFR3*, and their correlations with the clinicopathological variables are summarized in Table 2. No variables showed significant correlation with *FGFR3* mutations. Mutations were detected in six different codons. Mutations affecting the extracellular domain (exon 7) or transmembrane domain (exon 10) accounted for 95.8% (23/24) (Table 3). Intravesical recurrence was detected in 18 of 45 subjects (40%). The clinicopathological variables of the primary tumors, such as tumor stage, histological grade, tumor size, multiplicity, presence of carcinoma *in situ* lesion, and *FGFR3* mutational status, did not correlate with the intravesical recurrence (Table 4).

**Clinical usefulness of detecting *FGFR3* mutation in the urine sediments.** A total of 429 voiding urine samples were taken from 45 cases, among which 61 samples were preoperative urine samples consisting of 35 from recurrent and 26 from non-recurrent cases (Table 5). The remaining 368 urine samples were obtained serially during follow up, among which 93 samples were from recurrent cases and 275 samples were from non-recurrent cases. The concentrations of genomic DNA extracted from the urine samples were quantified in all samples prior to the assay. Of 429 urine samples, 114 (26.6%) were not available for the assay because their DNA concentrations were <0.125 ng/μL. A total of 315 samples (73.4%) were subjected to the *FGFR3* mutation detection assay. They were subjected to either the conventional PNA-mediated real-time PCR clamping assay or PPA method depending on their DNA concentrations.

**Risk of intravesical recurrence in patients showing *FGFR3* mutation in tumor tissues and urine sediments.** In 21 of 24 cases with *FGFR3* mutation in primary tumors, genomic DNA samples extracted from preoperative urine sediments before the initial TURBT were available for mutation detection assay. The sensitivity of *FGFR3* mutation in the urine samples was 62%

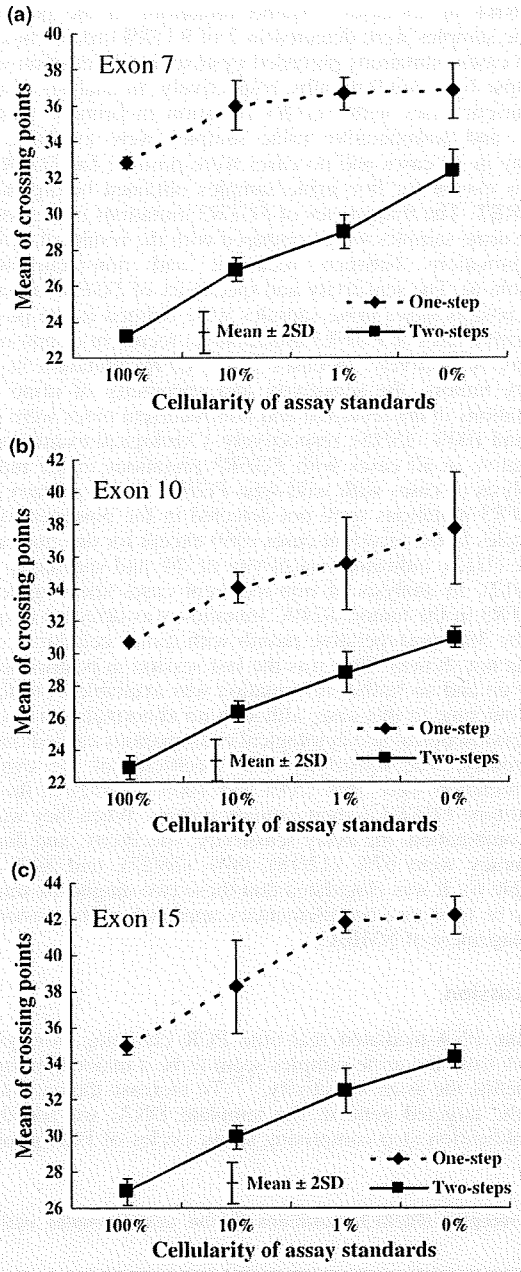


**Fig. 3.** Validation for sensitive detection of fibroblast growth factor receptor (*FGFR*)-3 mutation in trace amounts of the template DNA. (a) One nanogram of genomic DNA of four assay standards with 0, 1, 10, and 100% of tumor cellularity was amplified in octaplicate samples ($n$ = 8) under the conditions of the two-step assays comprising seven amplification cycles of the peptide nucleic acid (PNA)-free pre-amplifier, followed by PNA-mediated real-time PCR clamping for exon 7 of the *FGFR3* gene (solid lines). The data from the one-step assay are shown for comparison (dashed lines). The mean crossing points (CP) are plotted and the error bars represent 2 SD. Similar experiments were carried out to validate the assay protocols for (b) exon 10 and (c) exon 15.

(13/21), and their mutational types coincided with those of the primary tumors in all cases. In 21 cases showing wild-type *FGFR3* in primary tumor tissues, the preoperative urine samples were available for the assay in 13 cases and no mutations were found in these samples, showing the specificity of 100% (0/13). Tumor cellularities in the preoperative urine sediments were significantly higher in the recurrent cases than in the non-recurrent cases (Fig. 4a; $P$ = 0.008). An ROC curve analysis was performed to define the optimal cut-off value of tumor cellularity in the preoperative urine sediments. The area under the curve (AUC) was 0.847 (95% confidence interval, 0.669–1.026), and the cut-off value with optimal sensitivity and specificity was defined as 11% (Fig. 4b).

*FGFR3* mutational status in the primary tumors was not a significant predictor of intravesical recurrence after TURBT

**Table 2. Clinicopathological characteristics and fibroblast growth factor receptor (*FGFR*)-3 mutation status**

| Variables | Total | *FGFR3* status | | % of mutation | *P*-value |
|---|---|---|---|---|---|
| | | Wild-type | Mutation | | |
| Age (years) | | | | | |
| Mean ± SD | 63.0 ± 11.2 | 63.1 ± 12.7 | 62.8 ± 9.6 | – | 0.98 |
| Range | 36–80 | 36–80 | 45–78 | – | |
| Sex | | | | | |
| Male | 35 | 15 | 20 | 57 | 0.27 |
| Female | 10 | 6 | 4 | 40 | |
| Smoking history | | | | | |
| Present | 29 | 11 | 18 | 62 | 0.11 |
| Absent | 16 | 10 | 6 | 38 | |
| Tumor size (diameter, cm) | | | | | |
| <1 | 10 | 4 | 6 | 60 | 0.73 |
| 1–3 | 25 | 13 | 12 | 48 | |
| 3< | 10 | 4 | 6 | 60 | |
| Multiplicity | | | | | |
| Solitary | 27 | 12 | 15 | 56 | 0.71 |
| 2–3 | 12 | 5 | 7 | 58 | |
| ≥4 | 6 | 4 | 2 | 33 | |
| Pathological stage | | | | | |
| pTa | 19 | 7 | 12 | 63 | 0.26 |
| pT1 | 26 | 14 | 12 | 46 | |
| Tumor grade | | | | | |
| G1 | 6 | 3 | 3 | 50 | 0.97 |
| G2 | 35 | 16 | 19 | 54 | |
| G3 | 4 | 2 | 2 | 50 | |
| Concomitant CIS | | | | | |
| Present | 3 | 2 | 1 | 33 | 0.45 |
| Absent | 42 | 19 | 23 | 55 | |
| BCG therapy | | | | | |
| No | 40 | 19 | 21 | 53 | 0.87 |
| Treated | 5 | 2 | 3 | 60 | |
| Total | 45 | 21 | 24 | 53 | |

BCG, Bacille Calmette Guerin; CIS, carcinoma *in situ*.

**Table 3. Fibroblast growth factor receptor (*FGFR*)-3 mutational types detected in this study**

| *FGFR3* | Mutational type | | *n* | % |
|---|---|---|---|---|
| | Codon | Nucleotide | | |
| Exon 7 | R248C | CGC → TGC | 4 | 16.7 |
| | S249C | TCC → TGC | 8 | 33.3 |
| Exon 10 | G372C | GGC → TGC | 1 | 4.2 |
| | S373C | AGC → TGC | 1 | 4.2 |
| | Y375C | TAT → TGT | 9 | 37.5 |
| Exon 15 | K652E | AAG → GAG | 1 | 4.2 |
| Total | | | 24 | 100 |



doi: 10.1111/j.1349-7006.2009.01334.x

**Table 4. Correlation of the stage, histological grade, tumor size, multiplicity, concomitant CIS and fibroblast growth factor receptor (*FGFR*)-3 mutations in the tissue with intravesical tumor recurrence**

| Variables | Total | Recurrent | Non-recurrent | *P*-value* |
|---|---|---|---|---|
| No. subjects | 45 | 18 | 27 | |
| Stage | | | | |
| pTa | 19 | 8 | 11 | 1.00 |
| pT1 | 26 | 10 | 16 | |
| Grade | | | | |
| G1 | 6 | 1 | 5 | 0.43 |
| G2 | 35 | 15 | 20 | |
| G3 | 4 | 2 | 2 | |
| Tumor size (cm) | | | | |
| <3 | 35 | 12 | 23 | 0.14 |
| ≥3 | 10 | 6 | 4 | |
| Multiplicity | | | | |
| Solitary | 27 | 10 | 17 | 0.45 |
| Multiple | 18 | 8 | 10 | |
| Concomitant CIS | | | | |
| Absent | 42 | 16 | 26 | 0.25 |
| Present | 3 | 2 | 1 | |
| *FGFR3* mutations in the tumor tissues | | | | |
| Wild-type | 21 | 9 | 12 | 0.89 |
| Mutation | 24 | 9 | 15 | |

CIS, carcinoma *in situ*; *logrank test.

(Table 4). In cases harboring *FGFR3* mutations in the primary tumor, the levels of *FGFR3* mutations in the preoperative urine sediments significantly correlated with the 3-year recurrence-free survival rates (83.3 vs 22.2%) (Fig. 4c), whereas the results of preoperative urine cytology did not correlate with the recurrence-free survival.

**Serial determination of *FGFR3* mutations in the voided urine samples during the follow-up period after the initial TURBT.** *FGFR3* mutations in serially obtained urine samples were assayed quantitatively in the postoperative follow-up period. Low-copy number DNA samples were amplified by the PPA method using 1 ng of genomic DNA as the template. In 21 cases harboring *FGFR3* mutations in primary tumors, assay results were plotted on a 3-D line chart (Fig. 5). The preoperative sensitivities of urine *FGFR3* mutations in the recurrent and non-recurrent cases were 88.9% (8/9) and 41.7% (5/12), respectively. *FGFR3* mutations were not detected 1 month after the initial TURBT in all cases. *FGFR3* mutations in the postoperative urine samples were detected in 7 of 9 (78%) recurrent cases. In two cases, mutations preceded cystoscopical detection of tumor relapse by 6 and 9 months, respectively. In analysis of the non-recurrent cases with *FGFR3* mutation in primary tumors, the pre- and postoperative urine samples were available for the assay in 12 cases and no cases were positive for *FGFR3* mutations except for five urine samples obtained before the initial TURBT. The frequencies of *FGFR3* mutations in the postoperative urine samples were compared with the results of cytological examinations between recurrent and non-recurrent cases (Table 6). The sensitivity and specificity of *FGFR3* mutations in the postoperative urine samples were defined as the positive or negative rates of *FGFR3* mutations in recurrent or non-recurrent cases, respectively. In cases with *FGFR3* mutation in the primary tumors, the sensitivity and specificity of urine *FGFR3* mutations in the recurrent and non-recurrent cases were 78% (7/9) and 100% (15/15), respectively. Cytological examination was negative in all cases with *FGFR3* mutations in the tumors. In analysis of cases with wild-type *FGFR3* in the primary tumors, *FGFR3* mutations were not detected in the postoperative urine samples in the recurrent cases (0/9) except for one non-recurrent case (1/12), indicating sensitivity of 0% and specificity of 92% (11/12). In analysis of non-recurrent cases showing wild-type *FGFR3* in the tumor, S249C mutation was detected in one case at the 36th postoperative month with tumor cellularity of 2.1% (data not shown). This was the last session in postoperative follow up and no further information was available as to the clinical outcome in this case, although no abnormality was detected by cystoscopical and cytological examinations carried out simultaneously. The sensitivity and specificity of the cytological examination were 56% (5/9) and 100% (12/12) in those with wild-type *FGFR3* in their primary tumors. When they were used in combination, the assay sensitivity, specificity, and diagnostic accuracy were 67% (12/18), 96% (26/27), and 84% (38/45) (Table 6). It was elucidated that these two diagnostic modalities may be used as a complementary approach to the postoperative management of NMIBC.

## Discussion

In the PNA-mediated real-time PCR clamping, low yields of DNA from the urine samples seem to be a major limiting factor to define the assay sensitivity.[17] To increase the copy numbers of the targeted gene in the template DNA, we added a pre-amplification step comprising seven cycles of PCR prior to the

**Table 5. Correlation of DNA concentration and fibroblast growth factor receptor (*FGFR*)-3 mutations in the urine samples with tumor recurrence**

| Variables | Total | Recurrent | Non-recurrent | *P*-value |
|---|---|---|---|---|
| Collected urine samples | 429 | 128 | 301 | |
| Preoperative | 61 | 35† | 26 | |
| Follow-up | 368 | 93 | 275 | |
| DNA concentration (ng/μL) | | | | |
| Total | | | | |
| 50≦ | 83 (19.3%) | 23 (18.0%) | 60 (19.9%) | 0.885 |
| 0.125–50 | 232 (54.1%) | 71 (55.5%) | 161 (53.5%) | |
| 0.125< | 114 (26.6%) | 34 (26.6%) | 80 (26.6%) | |
| Mean ± SD (ng/μL) | 53.8 ± 187.6 | 36.2 ± 98.1 | 61.6 ± 214.3 | |
| Detection of *FGFR3* mutation in urine sediments | | | | |
| No. samples available for the assay | 315 | 94 | 221 | |
| Mutated | 26 (8.3%) | 20 (21.3%) | 6 (2.7%) | <0.0001 |
| WT | 289 (91.7%) | 74 (78.7%) | 215 (97.3%) | |

†Preoperative urine samples consisted of samples obtained in the initial transurethral resection of bladder tumor ($n$ = 18) and transurethral resection of bladder tumor for recurrence ($n$ = 17).